UNIVERSITY OF MINNESOTA
ST. ANTHONY FALLS LABORATORY
Engineering, Environmental and Geophysical Fluid Dynamics

Project Report No. 504

Shallow groundwater temperature response to urbanization and climate change in the Twin Cities Metropolitan Area: Analysis of vertical heat convection effects from the ground surface

by

Craig A. Taylor and Heinz G. Stefan

Prepared for

Minnesota Pollution Control Agency
St. Paul, Minnesota

May, 2008
Minneapolis, Minnesota

The University of Minnesota is committed to the policy that all persons shall have equal access to its programs, facilities, and employment without regard to race, religion, color, sex, national origin, handicap, age or veteran status.

Abstract

Groundwater temperatures, especially in shallow (quaternary) aquifers depend on ground surface temperatures which in turn depend on climate and land use. A key heat transfer processes that contributes to shallow groundwater temperatures is conduction from the soil surface into the groundwater. Groundwater temperatures therefore respond to ground surface temperatures. Ground surface temperatures have seasonal and diurnal cycles, and are modified by urban development, and climate change. In Minnesota seasonal temperature cycles penetrate the ground to depths on the order of 10 to 15m. In this report, we explore concepts and basic relationships by which groundwater temperatures are induced by conduction from the ground surface.

Our analysis indicates that a fully urbanized downtown area at the latitude of Minneapolis/St. Paul is likely to have a groundwater temperature that is nearly 3°C warmer than an undeveloped/ agricultural area. Pavements are the main cause of this change. Data collected by the MPCA in the St. Cloud, MN area confirm that land use influences groundwater temperatures.

Global warming will also result in a rise of ground surface temperatures and hence groundwater temperatures. In the extreme case of a $2xCO_2$ climate scenario groundwater temperatures would be expected to rise by up to 4°C.

Compounding urbanization and climate change, by applying the extreme $2xCO_2$ climate scenario to a land use change from “undeveloped” to “fully urbanized”, is expected to raise groundwater temperatures by about 5°C at the latitude of Minneapolis/St. Paul. A mean annual groundwater temperature rise of 5°C would likely have a very adverse affect on trout habitat in coldwater streams in summer.

Table of Contents

List of Terms

C = heat capacity (Sub-script denotes material)
d = mean grain size
$d\phi/dx$ = hydraulic gradient
k = hydraulic conductivity
k_o = overall heat transfer coefficient
L = zeroing phase shift
$M.C.$ = moisture content expressed as a percent of the dry weight of the soil
q_x = x-component flux
q_z = z-component flux
S = depth from the surface to the groundwater table
t = time
t_0 = period
T = soil temperature
T_m = mean temperature on the ground surface
T_s = temperature on the ground surface
T^*_R = soil or groundwater temperature with reflection at bedrock
U = Darcy velocity
$|V|$ = velocity magnitude
V_s, V_w, and V_a = volume fractions solids, water, and air respectively
v_x = x-component of velocity
v_z = z-component of velocity
z = depth below surface

α = thermal diffusivity
δ = damping factor
ΔT= amplitude of the temperature fluctuation on the ground surface
ΔT_f = fitted surface temperature amplitude
η = dynamic viscosity
φ = time-lag due to overall heat transfer coefficient
κ = thermal conductivity
λ = dimensionless lag
Λ = wavelength of one oscillation of temperature fluctuations
ρ = dry soil density

1. Introduction/Problem Description

Cold-water streams support a wide variety of fish populations, including several species of trout, salmon, and white bass. Groundwater (base flow) is the primary source of water for many cold-water streams. (Water released from deep reservoirs is another source). Urban development can influence groundwater temperatures in a number of ways: Paved surfaces become much warmer than sod surfaces on clear, sunny days (Figure 1.1a from Herb et al. 2006). Heat is conducted from these surfaces into the soil, and can reach shallow groundwater. Taniguchi and Uemura (2005) provide evidence of conduction based warming of groundwater due to urbanization. Surface water runoff from warm ground surfaces can infiltrate from ponds, channels, or rain gardens. Percolating warm water may carry its heat, not lost in the soil, into an aquifer.

Another cause of warmer ground temperatures is climate warming. Soil surface temperatures are likely to rise just as air temperatures are likely to get warmer, and heat conduction into the soil will increase ground temperatures. Evidence of such rise was provided by Baker and Baker (2002) and is reproduced in Figure 1.2.

The two readily identifiable processes of groundwater heating are heat transfer from a warm surface by conduction and the infiltration of warm water. Heat conduction will be particularly important for shallow aquifers with a water table close to the ground surface. Infiltration of warm water will be important for both shallow and deep aquifers. The main purpose of this report is to explore the connection between ground surface temperatures and groundwater temperatures by heat conduction and to estimate to potential warming of groundwater due to urbanization and global climate warming.

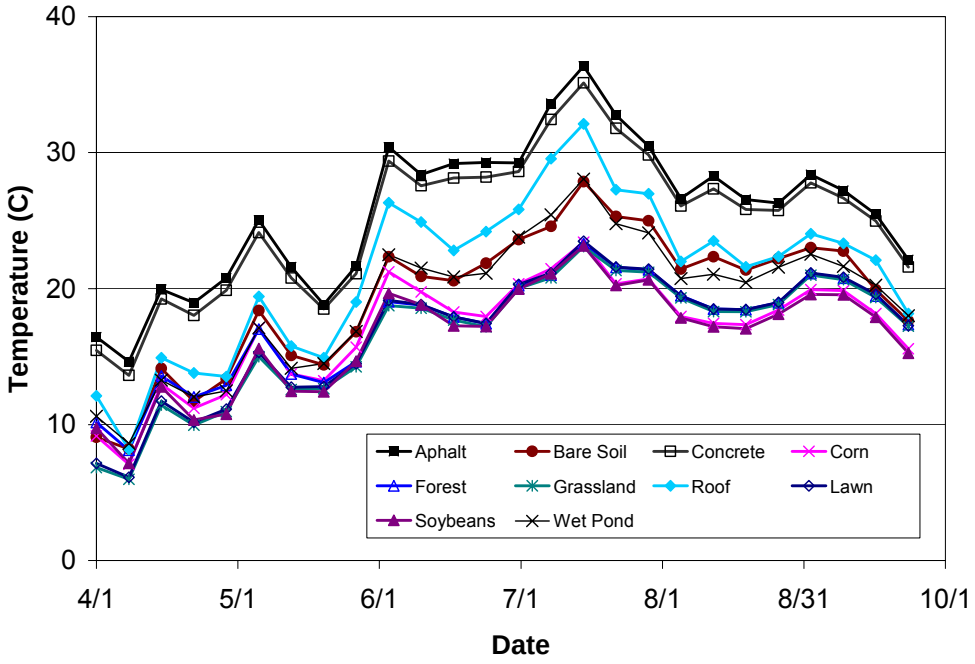

Figure 1.1. Simulated average weekly surface temperatures for ten land uses calculated with hourly climate data from St. Paul (2004) as model input (Herb et al. 2007).

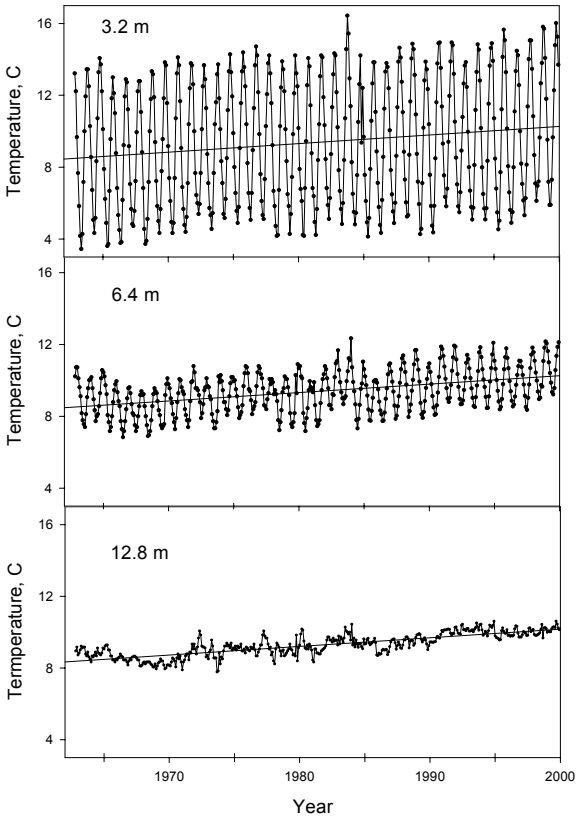

Figure 1.2. Trends in recorded ground temperatures in St. Paul, MN (Baker and Baker 2002)

2. Vertical heat conduction into soil

2.1 One-dimensional heat conduction equation and analytic solution for soil temperatures driven by periodic surface temperature fluctuations

Vertical heat condition from a uniform surface into unsaturated soil is a good starting point for our analysis because paved surfaces typically prevent infiltration, and at well-drained sites infiltration is of short duration after a rainfall event.

Ground surface temperatures are not constant. Daily (diurnal) and seasonal ground surface temperature cycles are common. In addition, random temperature fluctuations are superimposed. Diurnal temperature fluctuations will typically be seen at less than 1m depth in dry soil, but seasonal fluctuations may be detectable at depths of 10m or more.

The starting point of our analysis is the unsteady one-dimensional heat conduction equation given as equation (2.1). Baehr and Stephan (2006) provide an analytical solution of equation (2.1) for a semi-infinite solid with the boundary condition (2.2) at the z=0 boundary. Equation (2.2) represents a boundary temperature T_s that fluctuates with an amplitude ΔT and a period t_0 around a mean temperature T_m. The solution is equation (2.3), with parameters defined in equations (2.4) through (2.6). Note that some of the variables have been changed from Baehr and Stephan (2006) so that they would be more consistent with typical civil engineering notation.

$$\frac{\partial T}{\partial t} = \alpha \frac{\partial T}{\partial z} \tag{2.1}$$

$$T_s = T_m + \Delta T \cos\left(2\pi \frac{t}{t_0} \right) \tag{2.2}$$

$$T(z,t) = T_m + \Delta T \eta e^{-2\pi z/\Lambda} \cos\left(2\pi \left(\frac{t}{t_0} - \frac{z}{\Lambda} \right) - \varphi \right) \tag{2.3}$$

$$\Lambda = 2\sqrt{\pi \alpha t_0} \tag{2.4}$$

$$\varphi = \tan^{-1}\left(\frac{k_o}{1 + k_o} \right) \tag{2.5}$$

$$\frac{1}{\eta} = \sqrt{1 + 2k_o + 2k_o^{\,2}} \tag{2.6}$$

where T = soil temperature
T_s = temperature on the ground surface
T_m = mean temperature on the ground surface
ΔT= amplitude of the temperature fluctuation on the ground surface
z = depth below surface
t = time
t_0 = period
α = thermal diffusivity
Λ = wavelength of one oscillation of temperature fluctuations
k_o = overall heat transfer coefficient
φ = time-lag due to overall heat transfer coefficient
η = dynamic viscosity

The overall heat transfer coefficient, k_o, applies to the case where two fluids of different temperatures are separated by a wall at the boundary. The overall heat transfer coefficient takes into account the resistance to heat transfer in the wall and at the boundaries of the wall. In the case of heat conduction in soils, there is no resistance to heat transfer due to a wall or comparable object at

the surface. The overall heat transfer coefficient is, therefore, equal to zero. This results in ε = 0 and η = 1. Equation (2.2) can then be rewritten as

$$T(z,t) = T_m + \Delta T e^{-2\pi z/\Lambda} \cos\left(2\pi\left(\frac{t}{t_0} - \frac{z}{\Lambda}\right)\right). \quad (2.7)$$

When using equation (2.7) it is important to note the reference frame of the variable time. The first day of a 365 period does not fall on January 1st. The 365 day period starts with zero at the time of the warmest surface temperature. If it is desirable to have the first day of the period on January 1st, a correction term will have to be added to the cosine term in equation (2.7). This correction term would have to be adjusted on a case by case basis.

2.2 Damping factor and lag time

Equation (2.7) has two key components, a damping factor ($\delta = exp(-2\pi z/\Lambda)$) and a lag $\lambda = z/\Lambda$. The damping factor reduces the amplitude of the fluctuations as heat from the boundary is conducted deeper into the soil. The lag is the delay in time required for the surface temperature fluctuation to penetrate to a certain depth into the soil. Figure 2.1 provides a graph of the normalized damping factor, i.e. how the amplitude of the temperature fluctuation is reduced with depth in the soil. One can see that the temperature fluctuation is less than 1% of the ground surface value at a depth that equals about 15 wave lengths (Λ). Figure 2.2 shows an example of how the damping factor and lag change an idealized seasonal temperature fluctuation representative of St. Paul, MN, with depth. The surface temperature fluctuation of 26°C is still detectable at a depth of 8m, although it is reduced to less than 2°C.

The amplitude damping factor and the time lag depend heavily on the thermal diffusivity (α) of the soil. In turn, factors that affect the thermal diffusivity of soil include grain size, mineral composition, and moisture content. Appendix A provides a method of estimating the thermal diffusivity of soils based on the work of Kersten (1948) and De Vries (1966).

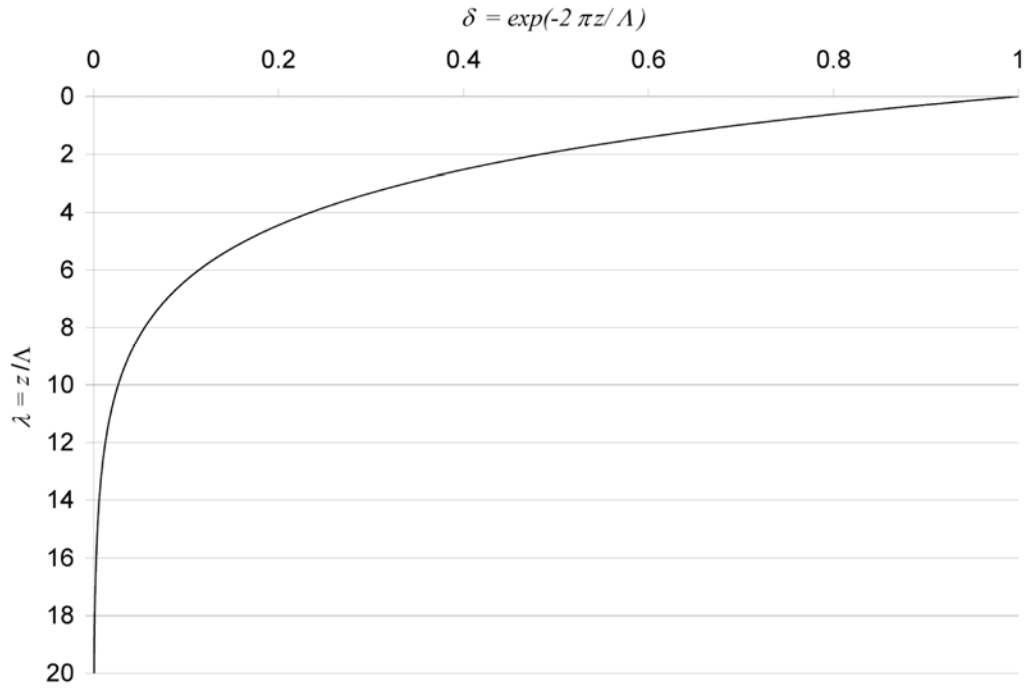

Figure 2.1. Damping of soil temperature amplitude δ with depth λ below the ground surface $z = 0$. The depth is normalized with Λ = oscillation wavelength of the temperature fluctuation in the soil (defined in Equ. 2.4)

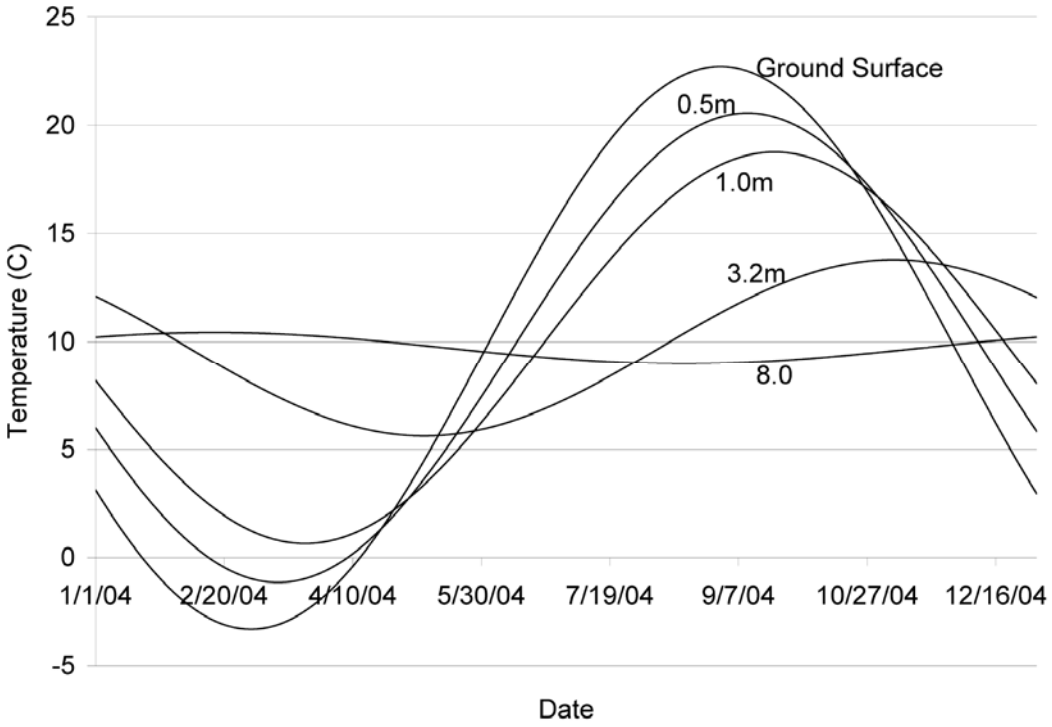

Figure 2.2. Example of computed seasonal heat (temperature) wave penetration, representative of St. Paul, MN

2.3 Data analysis

Data to verify equation (2.7) were obtained from a weather and soil temperature monitoring station at the University of Minnesota (St. Paul Campus Climatological Observatory). The observatory is maintained by the University of Minnesota's Department of Soil, Water and Climate and records soil temperature at various depths below a soded site and below a bare soil site (Data are also available for air temperature, solar radiation, precipitation, wind speed, pan evaporation, and several surface properties). Figures 2.3 and 2.4 give sample records from this site. The soil temperature is measured and continuously recorded beginning at a depth of about one centimeter and at sixteen additional depths down to a maximum of 11.2m.

In general, diurnal and seasonal ground surface temperature fluctuations can be approximated by a cosine curve with a 24-hour or 365-day period, respectively. The amplitudes differ by local climate (e.g. air temperature and cloudiness) and by land cover (e.g. grass or paved surface). For the St. Paul site the temperature record from 1cm depth was used as the boundary condition or surface temperature. An exact ground surface temperature on bare soil or grass is difficult to measure because many factors besides air temperature contribute to the temperature at the ground surface (Herb et al. 2006).

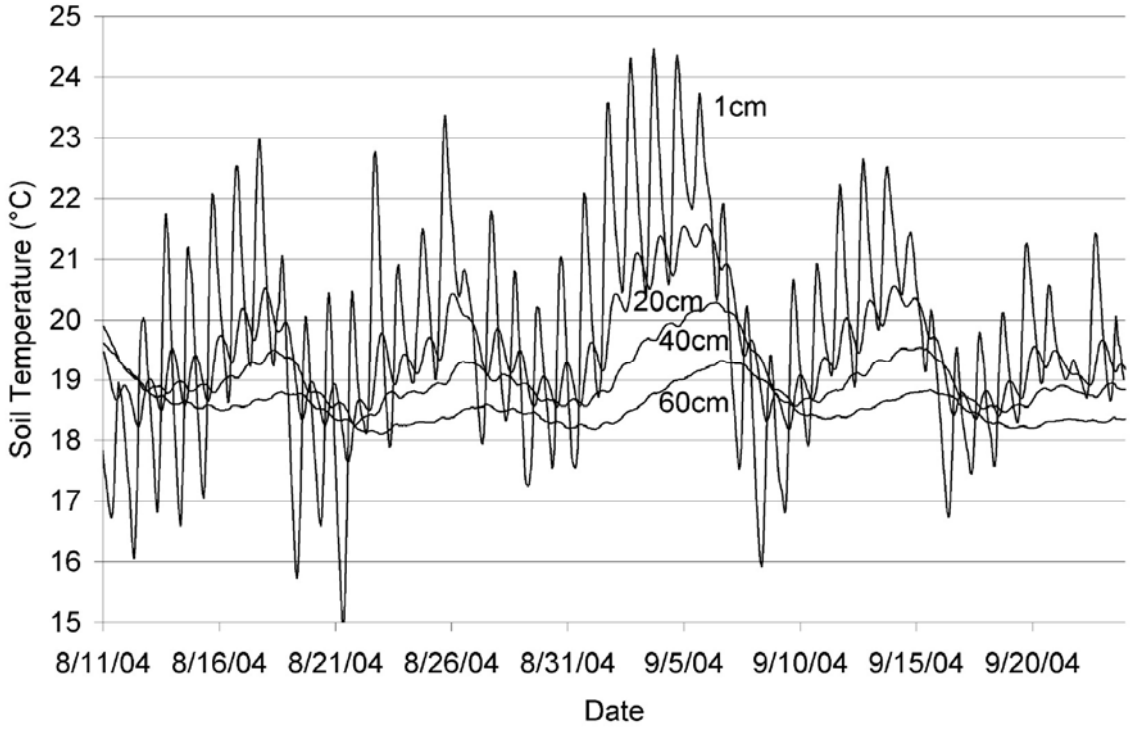

Figure 2.3 – Example of soil temperatures recorded below a soded ground surface at hourly intervals over 45 days (Depths measured in cm)

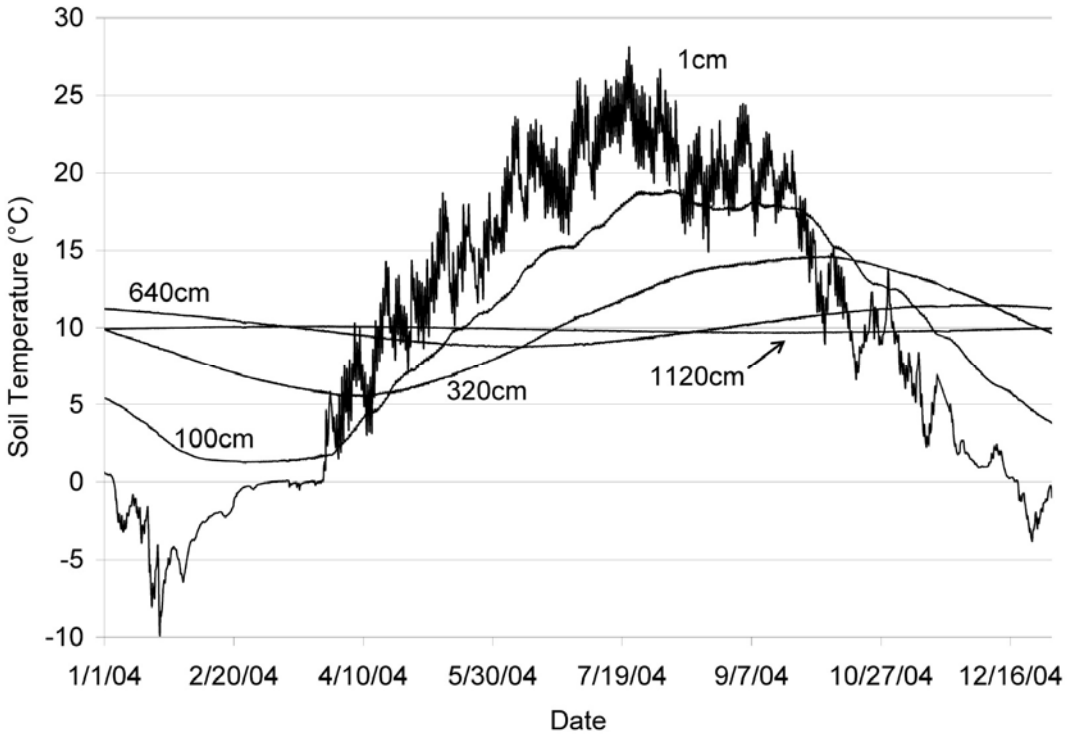

Figure 2.4. Example of soil temperatures recorded below a soded ground surface at hourly intervals over one year (depths measured in cm)

2.3.1 Seasonal soil temperature fluctuation amplitude and time lag

An example of a seasonal temperature fluctuation is given in Figure 2.4. Note that Figure 2.4 clearly shows the presence of both increasing amplitude damping with depth and increasing peak lag with depth.

A cosine curve, similar to equation (2.2) and (2.7), was fitted to the 2004 data at each depth at both sites. The data in this case were daily averages of hourly measurements. A phase shift (*L*) was added to the equations to match the unknown zero of the cosine curve to the zero of the seasonal data. With this phase shift added, equation (2.2) becomes equation (2.8), and equation (2.7), consequently, becomes equation (2.9).

$$T = T_m + \Delta T_f \cos\left(2\pi\left(\frac{t}{t_0} + L\right)\right) \tag{2.8}$$

$$T(z,t) = T_m + \Delta T e^{-2\pi z/\Lambda} \cos\left(2\pi\left(\frac{t}{t_0} + L - \frac{z}{\Lambda}\right)\right) \tag{2.9}$$

where ΔT_f = fitted surface temperature amplitude (^{o}C)

L = zeroing phase shift (-)

Knowing the fitted seasonal amplitude and the zeroing phase shift (L) at the ground surface (1cm depth), the amplitudes ($\Delta T e^{-2\pi z/\Lambda}$) and lags ($z/\Lambda$) can be obtained for all other depths by fitting equation (2.9) to the temperature data recorded at each depth. Tables 2.1 and 2.2 give the fitted seasonal amplitudes and lags, and the RMSE of the fitted curves.

The fitted phase shift at a depth of one centimeter is a consequence of "zeroing" the boundary condition only. The fitted phase shift at greater depths is due to both the zeroing of the boundary condition and the time lag due to conduction. Therefore, the actual lag at any depth below one centimeter is equal to the fitted phase shift at one centimeter minus the fitted phase shift at that depth. The modeled lag is equal to the depth (z) divided by the wavelength of one oscillation of temperature fluctuations (Λ). The amplitude is modeled by multiplying the fitted amplitude at a depth of 1cm with the damping factor for each depth.

Table 2.1 Sod-site seasonal soil temperature amplitude and time lag (phase shift) at different depths

Depth (m)	Fitted Amplitude (°C)	Fitted Phase Shift ( )	Fitted Phase Shift (days)	RMS Error (°C)
0.01	13.02	0.43	157.3	1.91
0.2	12.12	0.42	152.3	1.26
0.4	11.07	0.40	147.0	0.95
0.5	10.57	0.40	144.3	0.84
0.6	10.13	0.39	141.9	0.77
0.8	9.34	0.38	137.1	0.64
1	8.69	0.36	132.7	0.55
1.2	8.16	0.35	128.9	0.49
1.6	7.25	0.34	122.9	0.42
3.2	4.37	0.26	93.1	0.20
4.8	2.62	0.17	62.2	0.10
6.4	1.30	0.07	25.8	0.05
8	0.58	-0.05	-18.3	0.03
9.6	0.35	-0.13	-47.8	0.02
11.2	0.20	-0.21	-77.0	0.01

Table 2.2 Bare soil-site seasonal soil temperature amplitude and time lag (phase shift) at different depths.

Depth (m)	Fitted Amplitude (°C)	Fitted Phase Shift ( )	Fitted Phase Shift (days)	RMS Error (°C)
0.01	13.92	0.441	160.95	5.43
0.1	13.23	0.430	157.11	3.03
0.2	12.73	0.420	153.46	2.03
0.4	11.69	0.401	146.41	1.43
0.5	11.30	0.394	143.82	1.29
0.6	10.85	0.386	141.06	1.13
0.8	10.11	0.375	136.71	0.93
1.0	9.39	0.362	132.29	0.78
1.2	8.82	0.351	128.29	0.68

2.3.2 Soil thermal diffusivity from seasonal soil temperature amplitude and lag

A single thermal diffusivity for the soil column was determined by matching the observed (fitted) and the modeled (calculated) seasonal soil temperature amplitudes at depths from 0.2m to 11.2m. The soil temperature at the ground surface (1cm depth) was considered the forcing function. Thermal diffusivity (α) was considered optimal when the root-mean-square (RMS) of the differences between the observed and the modeled seasonal temperature amplitudes at all depths was at a minimum. Model input values used to compute the seasonal soil temperature amplitudes were: period t_0 = 365 days and L = 0.431. The optimized thermal diffusivity obtained from the amplitudes was α = 0.0624 m^2/day and the RMSE of the fitted soil temperature amplitudes was 0.23°C.

In a similar way, thermal diffusivity was also determined from the time lag of the seasonal temperature fluctuations that can be seen in Figures 2.2 and 2.4 for the modeled and the recorded soil temperature profiles, respectively. Model input values used to compute the seasonal soil temperature lag were: period t_0 = 365 days and L = 0.431. The optimized thermal diffusivity obtained from the time lag was α = 0.0651 m^2/day and the RMSE of the fitted seasonal time lags was 0.0095 or 3.47 days. Results for all soil layers are reported in Tables 2.3 and 2.4.

Table 2.3 Sod-site soil thermal diffusivities from seasonal soil temperature amplitude damping and lag

Depth (m)	Fit Amplitude (°C)	Damping Factor ( )	Model Amplitude (°C)	Amplitude Error** (%)	Fitted Phase Shift ( )	Fitted Lag* ( )	Fitted Lag* (day)	Model Lag ( )	Model Lag* (day)	Lag Error** (day)
0.01	13.0152	1.00			0.4310					
0.2	12.1150	0.93	12.0836	-0.26%	0.4172	0.0139	5.06	0.0116	4.23	-0.84
0.4	11.0748	0.86	11.2186	1.30%	0.4028	0.0282	10.30	0.0232	8.45	-1.85
0.5	10.5750	0.83	10.8097	2.22%	0.3953	0.0357	13.03	0.0289	10.56	-2.47
0.6	10.1299	0.80	10.4156	2.82%	0.3889	0.0422	15.39	0.0347	12.68	-2.71
0.8	9.3373	0.74	9.6701	3.56%	0.3757	0.0554	20.21	0.0463	16.90	-3.30
1	8.6916	0.69	8.9779	3.29%	0.3637	0.0674	24.60	0.0579	21.13	-3.47
1.2	8.1563	0.64	8.3353	2.19%	0.3531	0.0779	28.44	0.0695	25.35	-3.09
1.6	7.2521	0.55	7.1847	-0.93%	0.3366	0.0944	34.46	0.0926	33.81	-0.66
3.2	4.3693	0.30	3.9661	-9.23%	0.2551	0.1760	64.24	0.1852	67.61	3.37
4.8	2.6169	0.17	2.1894	-16.34%	0.1704	0.2607	95.14	0.2779	101.42	6.28
6.4	1.3039	0.09	1.2086	-7.31%	0.0706	0.3605	131.57	0.3705	135.22	3.65
8	0.5773	0.05	0.6672	15.57%	-0.0501	0.4811	175.60	0.4631	169.03	-6.58
9.6	0.3475	0.03	0.3683	5.99%	-0.1311	0.5621	205.18	0.5557	202.83	-2.35
11.2	0.1980	0.02	0.2033	2.66%	-0.2110	0.6421	234.36	0.6483	236.64	2.28

Notes: * Lag due to conduction
** Negative errors indicate a modeled value less than the fitted value

A similar analysis was done for a near by bare soil site. This using the amplitudes, the optimized thermal diffusivity obtained was α = 0.0539 with a RMSE = 0.16°C. Using the lag, the optimized thermal diffusivity obtained was α = 0.033 with a RMSE = 0.0053 or 1.94 days. The calculated diffusivities for the bare soil site are quite different despite having relatively low RMSEs. It should be noted that the calculations for the bare soil site are likely less accurate than the calculations for the sod site because the bare soil site has fewer data points. The higher error is shown in the higher RMSEs for the curving fittings in Table 2.2.

Table 2.4 Bare soil-site soil thermal diffusivities from seasonal soil temperature amplitude damping and lag

Depth (m)	Fitted Amplitude (°C)	Damping Factor ( )	Model Amplitude (°C)	Amplitude Error** (%)	Fitted Phase Shift ( )	Fitted Lag* ( )	Fitted Lag* (day)	Model Lag* ( )	Model Lag* (day)	Lag Error** (day)
0.01	13.9208	1.00			0.4410	0				
0.1	13.2313	0.96	13.3754	1.09%	0.4304	0.0105	3.84	0.0081	2.96	-0.88
0.2	12.7278	0.92	12.8514	0.97%	0.4204	0.0205	7.50	0.0162	5.92	-1.58
0.4	11.6930	0.85	11.8641	1.46%	0.4011	0.0399	14.55	0.0324	11.84	-2.70
0.5	11.2994	0.82	11.3993	0.88%	0.3940	0.0470	17.14	0.0406	14.80	-2.33
0.6	10.8491	0.79	10.9527	0.95%	0.3865	0.0545	19.90	0.0487	17.77	-2.13
0.8	10.1106	0.73	10.1113	0.01%	0.3745	0.0664	24.25	0.0649	23.69	-0.56
1	9.3914	0.67	9.3345	-0.61%	0.3624	0.0785	28.67	0.0811	29.61	0.94
1.2	8.8154	0.62	8.6175	-2.25%	0.3515	0.0895	32.67	0.0973	35.53	2.86

Notes: * Lag due to conduction
** Negative errors indicate a modeled value less than the fitted value

2.3.3 Diurnal soil temperature fluctuation amplitude

An example of recorded diurnal soil temperature fluctuations can be seen in Figure 2.3. Diurnal soil temperature fluctuations for 2004 were analyzed by the same method as the seasonal fluctuations, except that only the amplitudes were

considered. Each day's amplitude was calculated as one-half the difference between the recorded maximum and minimum hourly temperature.

Since it is to be expected that diurnal temperature fluctuations are driven by solar radiation, i.e. differences between day and night, temperature amplitudes recorded at 1cm depth were plotted against measured daily solar radiation (Figure 2.5). As expected there was a good correlation (Figure 2.6) for summer data (April to September), and a poor correlation for winter (January and February) because of snow cover and frozen soil conditions.

The averages of the recorded diurnal soil temperature amplitudes at the sod site over the summer months (April to September 2004) were used to compare observed and modeled damping of the diurnal soil temperature amplitudes with depth (Table 2.5). The following model values were used: period t_0 = 1 day and Λ = 0.885. A thermal diffusivity α = 0.0623 m^2/day for the soil layer from 0.1 to 0.5m depth gave the best match; the RMSE between the fitted and the observed diurnal soil temperature amplitude at all depths from 0.1 to 0.5m was 0.022^{o}C.

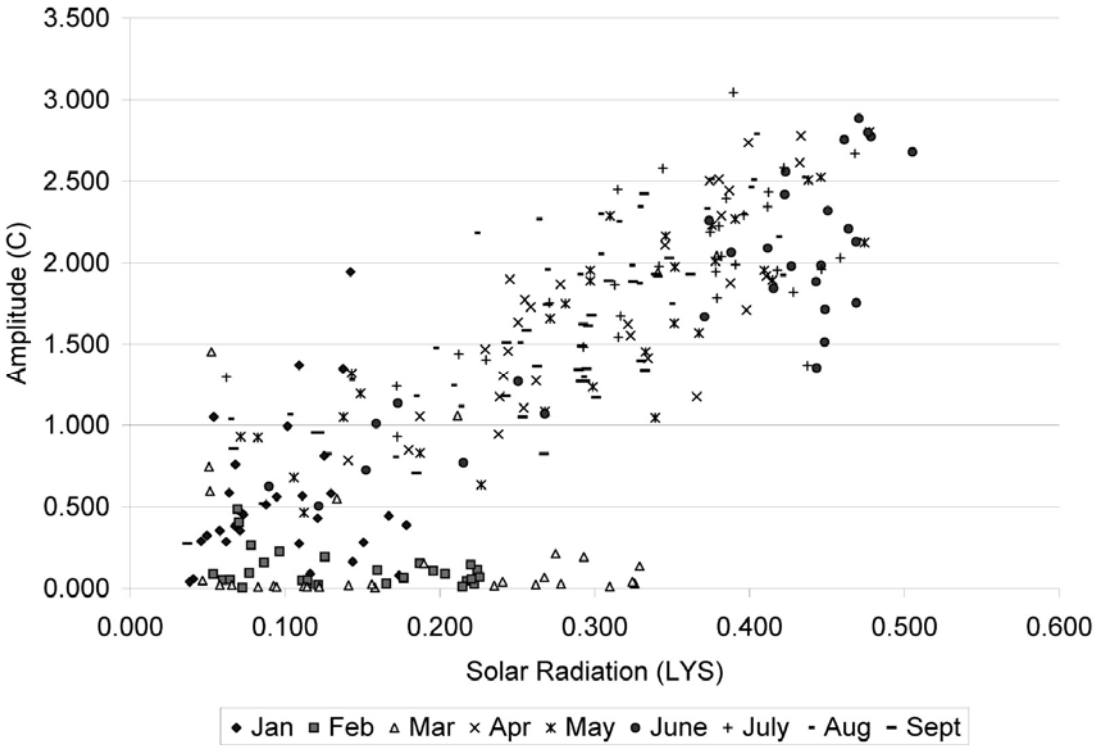

Figure 2.5. Diurnal soil temperature amplitude at 1 cm depth vs. total daily radiation for all available months in 2004 (Jan – Sept)

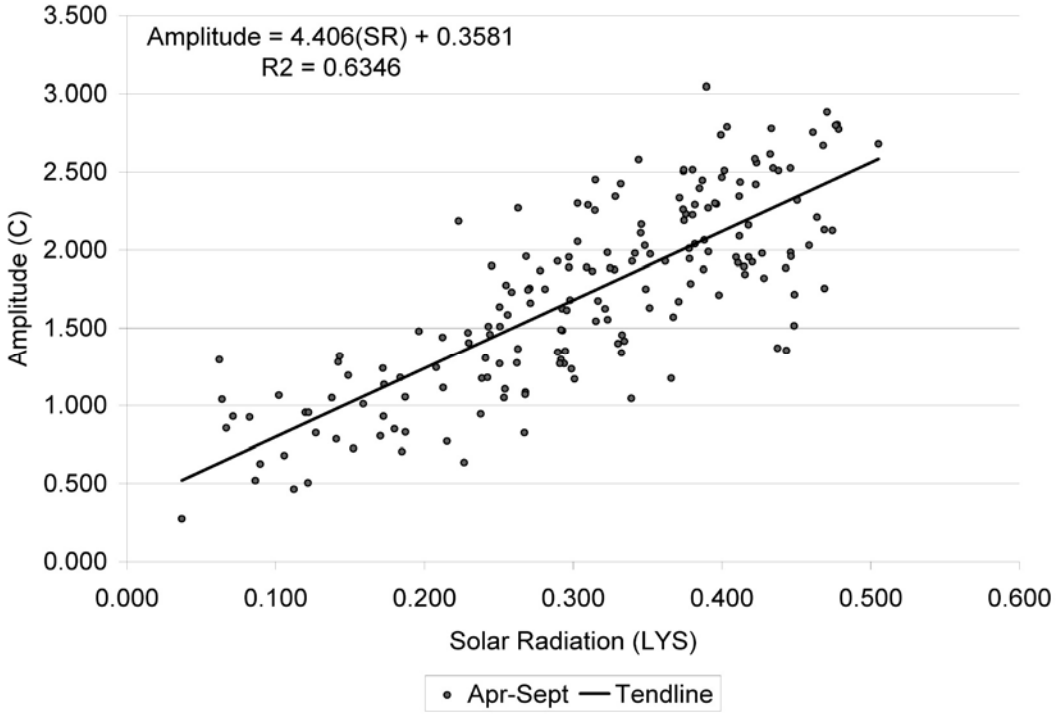

Figure 2.6. Diurnal soil temperature amplitude at 1 cm depth vs. total daily radiation in the summer months (Apr -Sept 2004)

Table 2.5 Sod-site average diurnal soil temperature amplitude (April-Sept 2004) at different depths

Depth (m)	Net Depth (m)	Average Amplitude (°C)	Model Amplitude (°C)	Amplitude Difference (°C)
0.01	0	1.7246		
0.05	0.04	1.2875	1.2983	-0.0108
0.10	0.09	0.8955	0.9103	-0.0148
0.20	0.19	0.4487	0.4476	0.0011
0.40	0.39	0.1481	0.1082	0.0399
0.50	0.49	0.1139	0.0532	0.0607

Notes: * Negative errors indicate a modeled value less than the fitted value

2.3.4 Penetration depth of ground surface temperature fluctuations

The penetration of ground surface temperature fluctuations into the soil is of special interest. Seasonal and diurnal soil temperature fluctuations have vastly different penetration depths. The plot in Figure 2.7 illustrates the computed penetration of seasonal ground surface temperature fluctuations into the soil. The plot was generated from Equ. (2.7) with a mean annual temperature T_m =

9.71. Diurnal temperature fluctuations in most soils are expected to be negligible at depths greater than 0.5 m. For example, at a depth of 0.5 m with a ground surface temperature amplitude ΔT = 13.02°C and a thermal conductivity α = 0.0656m^2/day the diurnal temperature fluctuation according to Table 2.5 is quite small (0.11°C).

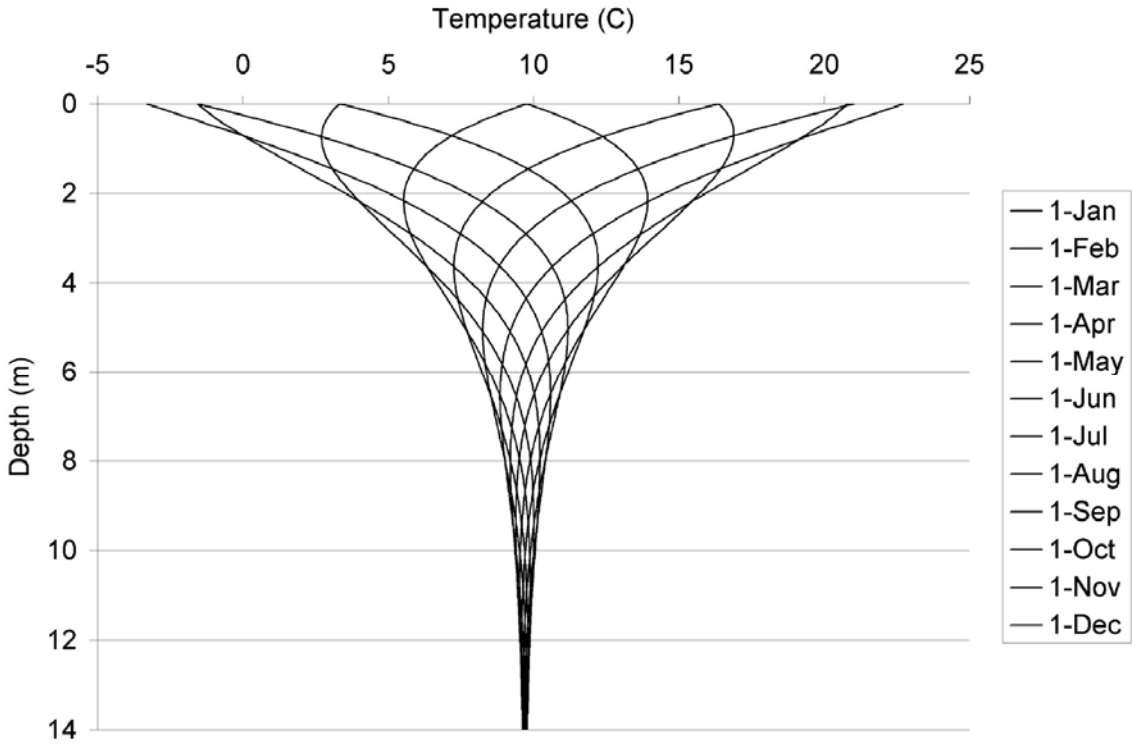

Figure 2.7. Example of computed monthly temperature profiles in the soil (representative of St. Paul, MN).

Figure 2.8 is a normalized version of Figure 2.7 and similar to a plot by Baehr and Stephan (2006). Figure 2.8 can be used for any mean annual temperature, any seasonal ground surface temperature fluctuation and any thermal diffusivity. According to Figure 2.8 the normalized temperature fluctuation penetrates to a depth of no more than $z/\Lambda \approx 0.8$. At that depth the temperature fluctuation will be less than 1% of the temperature amplitude ΔT at the ground surface. With $\Lambda = 2\sqrt{\pi \alpha t_0}$ from Equ 2.4, the diurnal and the seasonal penetration depths can be calculated with t_0 = 1 day and t_0 = 365 days, respectively. For a thermal diffusivity α = 0.065 m^2/day, representative of the St. Paul site, the diurnal penetration depth is 0.90 m, and the seasonal penetration depth is 13.8m.

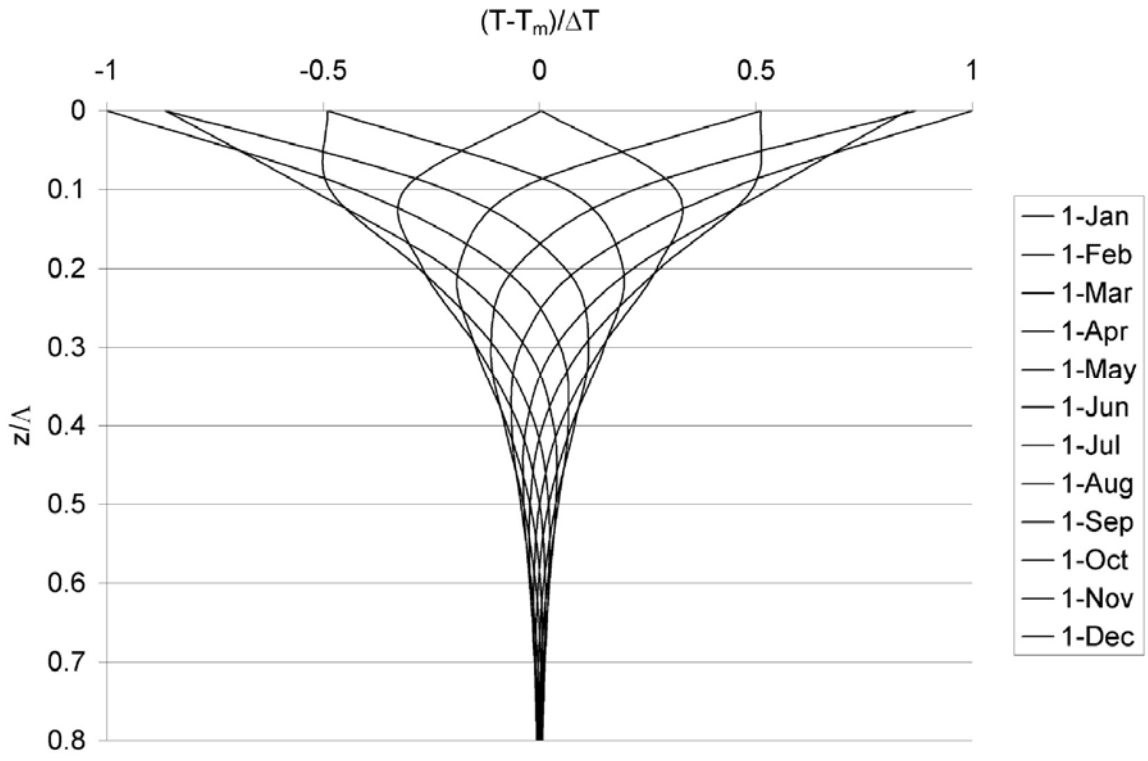

Figure 2.8. Example of normalized computed seasonal temperature fluctuation penetration (representative of St. Paul, MN).

3. Vertical heat conduction into shallow groundwater

As demonstrated in the previous section, seasonal temperature fluctuations at the ground surface can penetrate several meters deep into the soil. Surface temperature fluctuations can therefore also penetrate into shallow groundwater below the ground surface. The presence of standing or flowing groundwater in the soil pores, i.e. the presence of an aquifer, greatly increases the thermal diffusivity. Groundwater in an aquifer of low permeability (small grain sizes and low flow velocities) increases thermal diffusivity primarily by replacing the air in the pore spaces. In an aquifer of high permeability (large particle sizes and high flow velocities), hydrodynamic effects further increase the thermal diffusivity and hence the rate of heat transport. With increasing flow velocity of the water in the pore system, inertial effects and eventually turbulence raise the apparent thermal diffusivity until it is orders of magnitude greater then molecular thermal diffusivity. The dependency of diffusivity on flow has been studied extensively for mass transport in porous media, and the results are also applicable to heat transfer because of the Reynolds' analogy. A review of hydrodynamic diffusion/dispersion is given in Appendix B. It should be noted that water vapor and evaporation can transport significant amounts of heat in the unsaturated zone (Asaeda and Ca 1993), but this mechanism will not be included in this analysis.

The governing equation for vertical heat conduction in an aquifer (groundwater) is the same as for soil, except that the effective thermal diffusivity changes at the groundwater table (interface of unsaturated soil and groundwater). The difference between the thermal diffusivity of the unsaturated soil above the groundwater table (α_s) and the thermal diffusivity in the aquifer (α_g) adds a new parameter to the problem: the thermal diffusivity ratio (α_g/α_s). Expected values of this ratio will be from 1 to 1000.

Figure 3.1 shows a diagram of an aquifer of thickness h on top of an impervious bedrock or clay layer, and below an unsaturated soil layer of depth S, This 1-D system will be analyzed. The ground surface temperatures will be assumed to be uniform in horizontal direction, but fluctuating periodically in time; this assumption was also made in the analysis of the unsaturated soil in the previous section of this report.

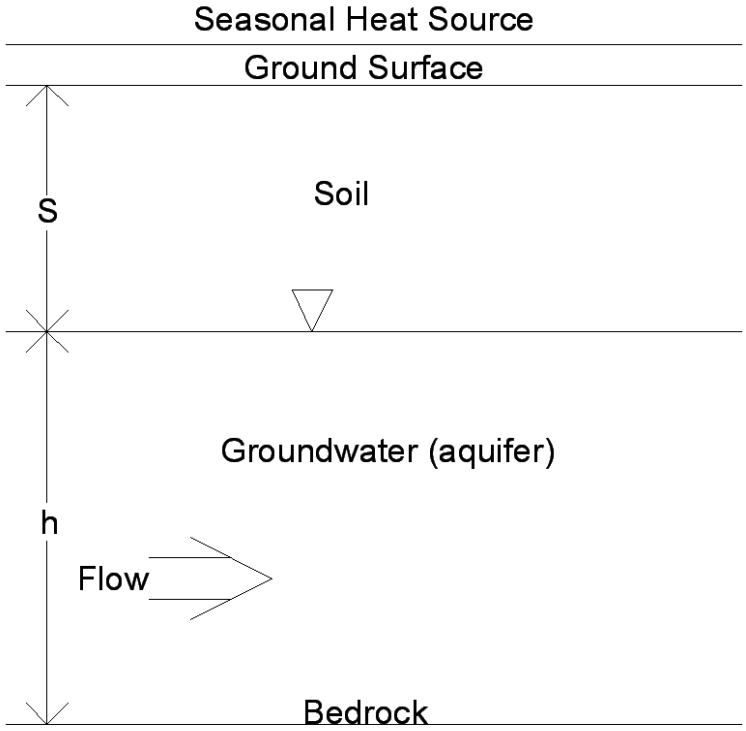

Figure 3.1. Schematic of aquifer of thickness h at depth S below the ground surface

It is temping to apply the solutions given in the previous section for a uniform soil to describe the vertical temperature profile in the groundwater. There are two methods by which this is typically done: 1) mapping or warping the depth term (z) to account for the change in diffusivity and 2) by using the solution of the unsaturated soil problem at the groundwater table as a boundary condition for the solution in the aquifer domain. Both of these methods produce the same

results and both are correct for steady-state heat transfer, but incorrect for unsteady heat transfer. The higher diffusivity in the aquifer increases the heat flux across the groundwater table. When solving for the temperature in the unsaturated soil, the analytic solution works from the top down and does not account for the increased heat flux and heat storage in the aquifer layer. For the unsteady heat transfer process the resistance for the vertical heat flux into the aquifer becomes concentrated in the overlying unsaturated soil layer. The unsteady analytic solution by mapping or warping underestimates the damping in the unsaturated soil layer and therefore gives incorrect groundwater temperatures. Appendix C applies the boundary condition translation scheme to determine an analytic solution and provides an example of how greatly the damping can be underestimated.

3.1 Numerical solution for vertical heat conduction into shallow groundwater

Using a numeric solution the governing equation (2.1) can be solved directly. By using a dimensionless form of the governing equation a more general solution can be provided. The governing equation given in equation (2.1) has an upper cosine boundary condition given in equation (2.2). For the lower boundary an adiabatic boundary condition is used (dT/dz = 0). In order to develop a dimensionless form of the governing equation, the following dimensionless variables are defined:

$$T^* \equiv \frac{T - T_m}{\Delta T}$$

$$t^* \equiv \frac{t}{t_0}$$

$$z^* \equiv \frac{z}{S}$$

where: S = depth from the surface to the groundwater table

Substituting these dimensionless variables into the governing equation yields

$$\frac{\Delta T}{t_0}\frac{\partial T^*}{\partial t^*} + \frac{1}{t_0}\frac{\partial T_m}{\partial t^*} = \frac{\alpha \Delta T}{S}\frac{\partial T^*}{\partial z^*} \qquad (3.1)$$

Since the mean surface temperature is not time dependant, the second them on the left hand side is equal to zero. Given this simplification equation (3.1) becomes:

$$\frac{\partial T^*}{\partial t^*} = \alpha^* \frac{\partial T^*}{\partial z^*} \tag{3.2}$$

where: $\alpha^* \equiv \frac{\alpha \cdot t_0}{S}$ is a unitless diffusivity

Applying the new dimensionless variables the boundary conditions at the ground surface and at the bottom of the aquifer can be written, respectively, as:

$$T^* = \cos\left(2\pi \cdot t^*\right) \tag{3.3}$$

$$\frac{\partial T^*}{\partial z^*} = 0 \tag{3.4}$$

The solution of the dimensionless governing equation is complicated by the diffusivity changing across the groundwater table. A numerical solution of equation (3.2) is therefore developed. The changing diffusivity across the groundwater table is addressed by breaking the domain of z^* into three sub-domains: the unsaturated soil, the water table, and the groundwater. In the unsaturated soil and in the groundwater the dimensionless governing equation is discretized using the Crank-Nicolson method discussed by Hoffmann and Chiang (2004). The discretized version of equation (3.2) for the unsaturated soil and groundwater zone is provided in equation (3.5), where $\alpha^* = \alpha^*_s$ for the unsaturated soil and $\alpha^* = \alpha^*_g$ for the groundwater.

$$\frac{T_k^{*n+1} - T_k^{*n}}{\Delta t^*} = \frac{\alpha^*}{2}\left[\frac{T_{k+1}^{*n+1} - 2T_k^{*n+1} + T_{k-1}^{*n+1}}{\Delta z^*} + \frac{T_{k+1}^{*n} - 2T_k^{*n} + T_{k-1}^{*n}}{\Delta z^*}\right] \tag{3.5}$$

where: n = denotes the time step number
T = denotes the z-direction step number

The discretization of equation (3.2) at the groundwater table is similar to the Crank-Nicolson method used in equation (3.5); however, at the groundwater table α^*_g is used for the terms entering the groundwater and α^*_s is used for terms entering the unsaturated soil, resulting in equation (3.6).

$$\frac{T_k^{*n+1} - T_k^{*n}}{\Delta t^*} = \frac{1}{2}\left[\frac{\alpha_g^*\left(T_{k+1}^{*n+1} - T_k^{*n+1}\right) + \alpha_s^*\left(T_{k-1}^{*n+1} - T_k^{*n+1}\right)}{\Delta z^*} + \frac{\alpha_g^*\left(T_{k+1}^{*n} - T_k^{*n}\right) + \alpha_s^*\left(T_{k-1}^{*n} - T_k^{*n}\right)}{\Delta z^*}\right] \tag{3.6}$$

The discretized equations (3.5) and (3.6) require implicit solutions and are second order accurate in both time and space. By gathering the n+1 terms on the left-hand side, a tridiagonal matrix can be developed to solve for the entire temperature profile for each time step. The matrix is given by the generic equation:

$$A \cdot T_{k-1}^{*n+1} + B \cdot T_k^{*n+1} + C \cdot T_{k+1}^{*n+1} = rhs \tag{3.7}$$

where for the unsaturated zone and for the groundwater:

$$A = C \equiv \frac{-\alpha^* \Delta t^*}{2\Delta z^{*2}}$$

$$B \equiv 1 + \frac{\alpha^* \Delta t^*}{\Delta z^{*2}}$$

$$rhs \equiv T_k^{*n} + \frac{\alpha^* \Delta t^*}{2\Delta z^{*2}} \left(T_{k+1}^{*n} - 2T_k^{*n} + T_{k-1}^{*n} \right)$$

and for the groundwater table:

$$A \equiv \frac{-\alpha_s^* \Delta t^*}{2\Delta z^{*2}}$$

$$B \equiv 1 + \frac{\Delta t^*}{2\Delta z^{*2}} \left(\alpha_s^* + \alpha_g^* \right)$$

$$C \equiv \frac{-\alpha_g^* \Delta t^*}{2\Delta z^{*2}}$$

$$rhs \equiv T_k^{*n} + \frac{\Delta t^*}{2\Delta z^{*2}} \left[\alpha_g^* \left(T_{k+1}^{*n} - T_k^{*n} \right) + \alpha_s^* \left(T_{k-1}^{*n} - T_k^{*n} \right) \right]$$

For any time step the boundary condition at the ground surface is a known temperature determined by equation (3.3). For the boundary condition at the bottom of the aquifer, Hoffmann and Chiang (2004) introduce a fictitious boundary that facilitates a second order accurate central difference discretization, which yields:

$$\frac{\partial T^*}{\partial z^*} = \frac{T_{k_{MAX}+1}^{*n+1} - T_{k_{MAX}-1}^{*n+1}}{2 \cdot \Delta z^*} = 0$$

$$\Rightarrow T_{k_{MAX}+1}^{*n+1} = T_{k_{MAX}-1}^{*n+1}$$

where k_{MAX}-1 denotes the point one step above the lower boundary
k_{MAX}+1 denotes an imaginary point one step below the lower boundary

Equation (3.7) and the lower boundary condition result in the following tridiagonal matrix:

$$\begin{bmatrix} B_2 & C_2 & & & & & \\ A_3 & B_3 & C_3 & & & & \\ & A_4 & B_4 & B_4 & & & \\ & & \ddots & \ddots & \ddots & & \\ & & & \ddots & \ddots & \ddots & \\ & & & & A_{k_{MAX}-1} & B_{k_{MAX}-1} & C_{k_{MAX}-1} \\ & & & & & A_{k_{MAX}}+C_{k_{MAX}} & B_{k_{MAX}} \end{bmatrix} \begin{bmatrix} T_2^{*n+1} \\ T_3^{*n+1} \\ T_4^{*n+1} \\ \vdots \\ \vdots \\ T_{k_{MAX}-1}^{*n+1} \\ T_{k_{MAX}}^{*n+1} \end{bmatrix} = \begin{bmatrix} rhs_2 - A_2 \cdot T_1^{*n+1} \\ rhs_3 \\ rhs_4 \\ \vdots \\ \vdots \\ rhs_{k_{MAX}-1} \\ rhs_{k_{MAX}} \end{bmatrix}$$

This tridiagonal matrix can be numerically solved quite efficiently. Tridiagonal matrix solver algorithms are readily available for most programming languages. The upper boundary condition is cyclical. This means that the initial condition throughout the rest of the domain is arbitrary because its effect on the solution will diminish over long enough time spans. The analytical model presented in Appendix C was used as an initial condition. The model was then run for 30 cycles (years) and only the last year was retained as the solution to the governing equation.

Example: An example (application) is provided in Figure 3.2. The following site properties have been used: S = 2.0m, h = 40.0m, α_s = 0.07 m^2/day, α_g/α_s = 5, T_m = 10.1 °C and ΔT = 13.1°C.

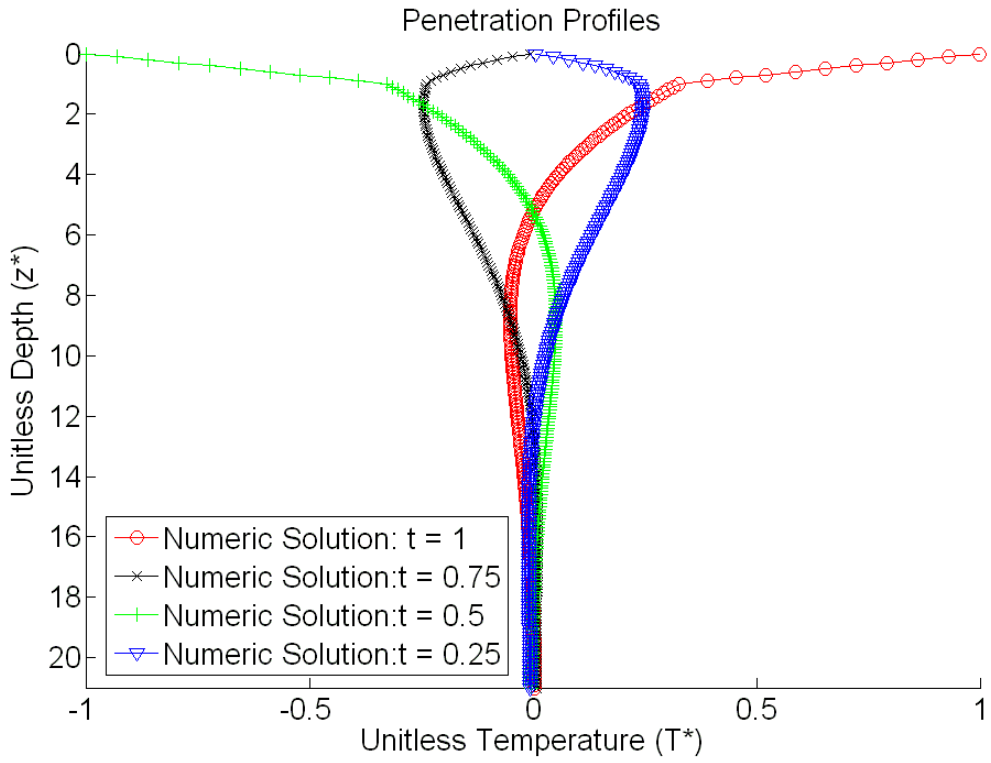

Figure 3.2a - Example of computed seasonal soil and ground water temperature profiles at the quarter points of a seasonal temperature cycle. Soil layer thickness S=2m; thermal diffusivities in the soil α = 0.07 m^2/day (representative of the St.

Paul, MN, site); in the aquifer α = 0.35 m^2/day; mean surface temperature and surface amplitude are T_m = 10.1 °C and ΔT = 13.1 °C, respectively (both representative of the St. Paul, MN, sod site); aquifer depth h = 40m. Unitless depths z* = z/S, and unitless temperatures T* = (T-T_m) / ΔT.

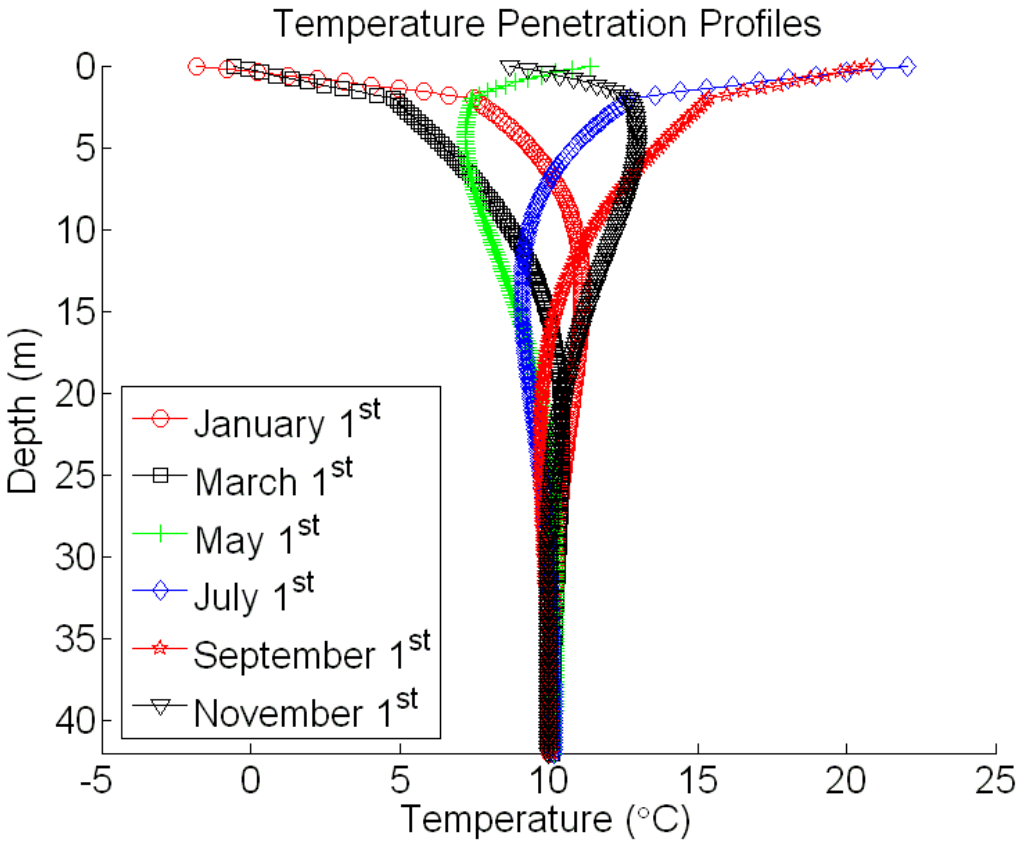

Figure 3.2b- Example of computed seasonal soil and ground water temperature profiles at the beginning of March, May, July and September. Soil layer thickness S=2m; thermal diffusivities in the soil α = 0.07 m^2/day (representative of the St. Paul, MN, site); in the aquifer α = 0.35 m^2/day; mean surface temperature and surface amplitude are T_m = 10.1 °C and ΔT = 13.1 °C, respectively (both representative of the St. Paul, MN, sod site); aquifer thickness h = 40m.

3.2 Numerical results for vertical heat conduction into shallow groundwater

Using the solution method presented in section 3.1, the one-dimensional heat conduction into a shallow groundwater can be analyzed for a wide range of field conditions, including different thermal diffusivities, different soil/aquifer depths, and different ground surface temperature regimes. Before conducting such an analysis it would be valuable to first determine if the groundwater temperature fluctuations are great enough to be of concern. Since groundwater temperature fluctuations (seasonal amplitudes) are greatest at the groundwater

table, Figure 3.3 has been included to determine the damping factor at the groundwater table for a range of dimensionless soil diffusivities and diffusivity ratios. The maximum range of seasonal groundwater temperatures can be found by multiplying the damping factor (δ) by twice the surface temperature amplitude (ΔT).

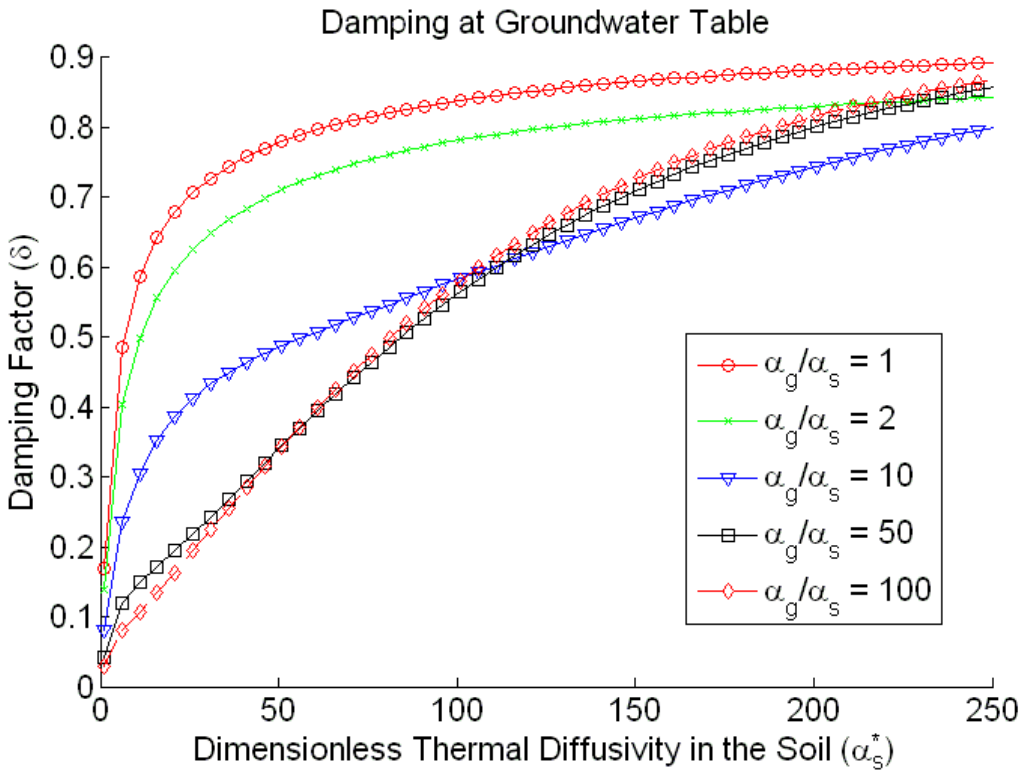

Figure 3.3 – Damping factor (δ) of the seasonal temperature amplitude at the groundwater table for an aquifer of infinite thickness

It would be impractical to plot temperature profiles or provide temperature tables for all imaginable values. Instead three typical values of unitless soil thermal diffusivity α^*_s, where $\alpha^*_s \equiv \frac{\alpha_s \cdot t_0}{S}$, were chosen and plots of seasonal temperature amplitude damping δ (Figures 3.4a-e) and of time lag λ (Figure 3.5a-e) were generated for various ratios of α^*_g / α^*_s. The two parameters δ and λ were plotted versus depth in normalized form. The unitless depth is $z^*=z/S$, seasonal temperature amplitude $\Delta T(z^*)$ at depth z^* is normalized against the seasonal ground surface temperature amplitude ΔT at $z^*=0$. The time lag is normalized against the period $t_0 = 365$ days of the seasonal temperature fluctuation. In order to generate the numerical values for damping and lag plotted in Figures 3.3 and 3.4,, the model discussed in section 3.1 was run for 30 years using a time step Δt^* = 0.001 and a depth step Δz^* = 0.1.

Using the damping and lag plots the temperature at any depth and time can be determined for each of the given unitless diffusivities using equation (3.8). Recall that the zero time occurs when the temperature is highest. If it is desired that the zero time fall on January 1st, then an appropriate phase shift should be added to equation (3.8).

$$T^* = \delta \cos\left(2\pi\left(t^* - \lambda\right)\right) \tag{3.8}$$

where: δ = damping factor

λ = dimensionless lag

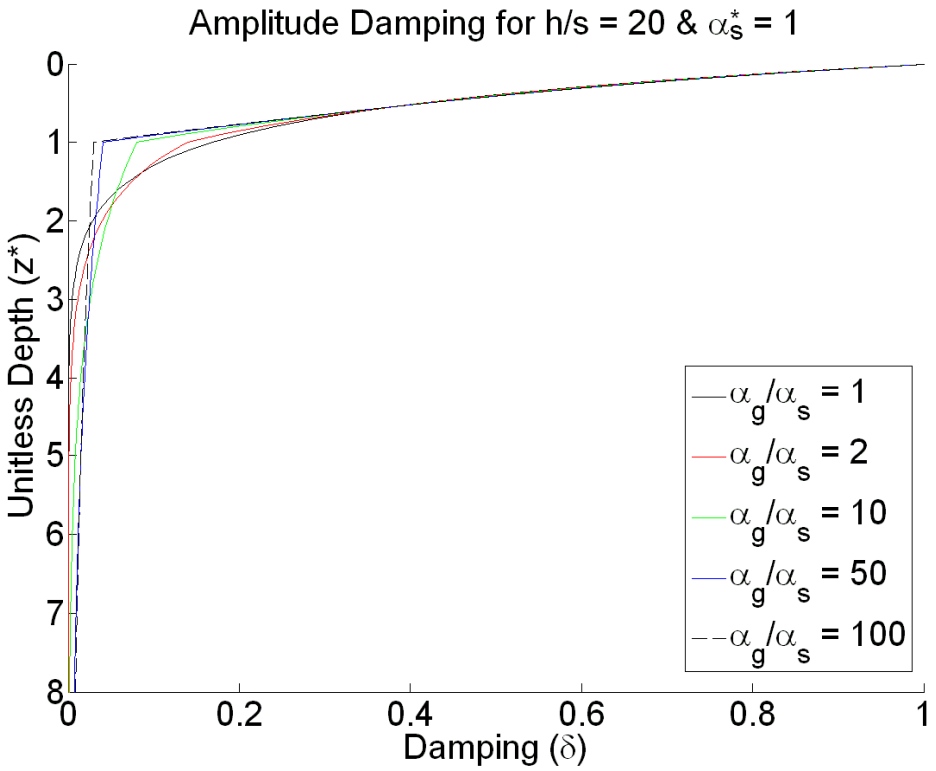

Figure 3.4a – Damping factor (δ) for α^*_s = 1.0 and *h/s* = 20

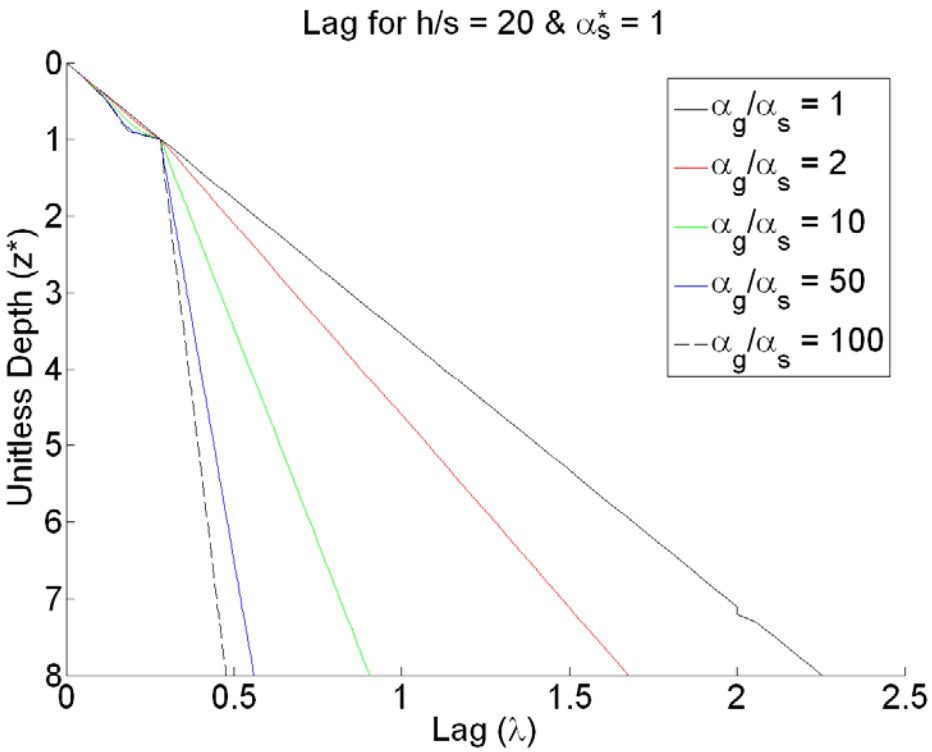

Figure 3.5a – Lag (λ) for α^*_s = 1.0

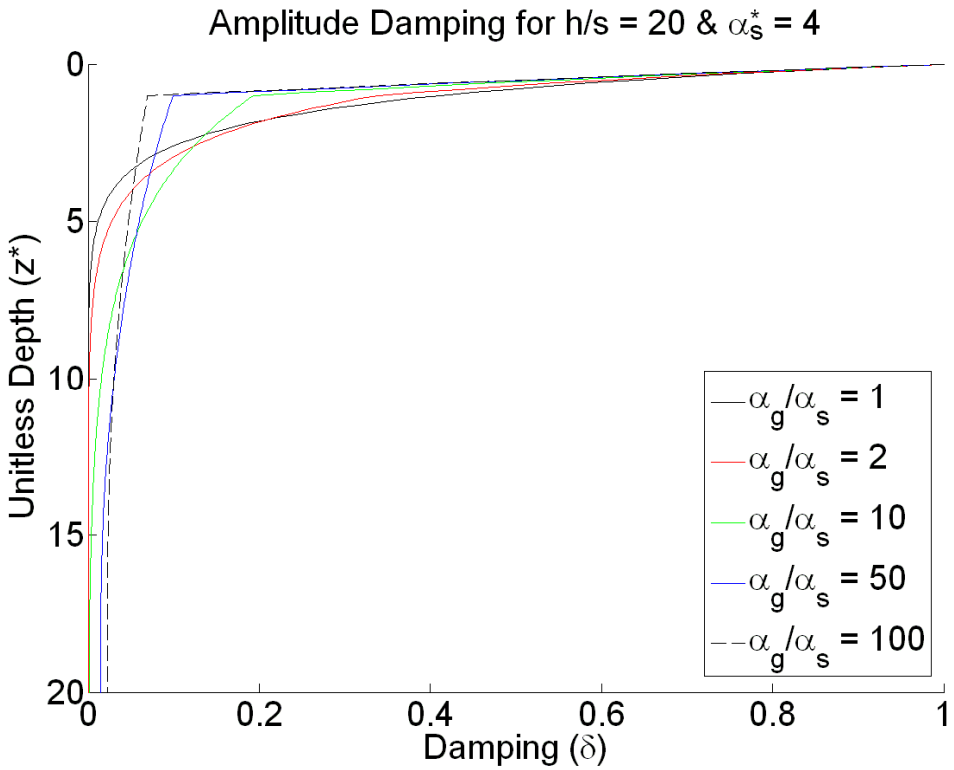

Figure 3.4b – Damping factor (δ) for α^*_s = 4.0 and *h/s* = 20

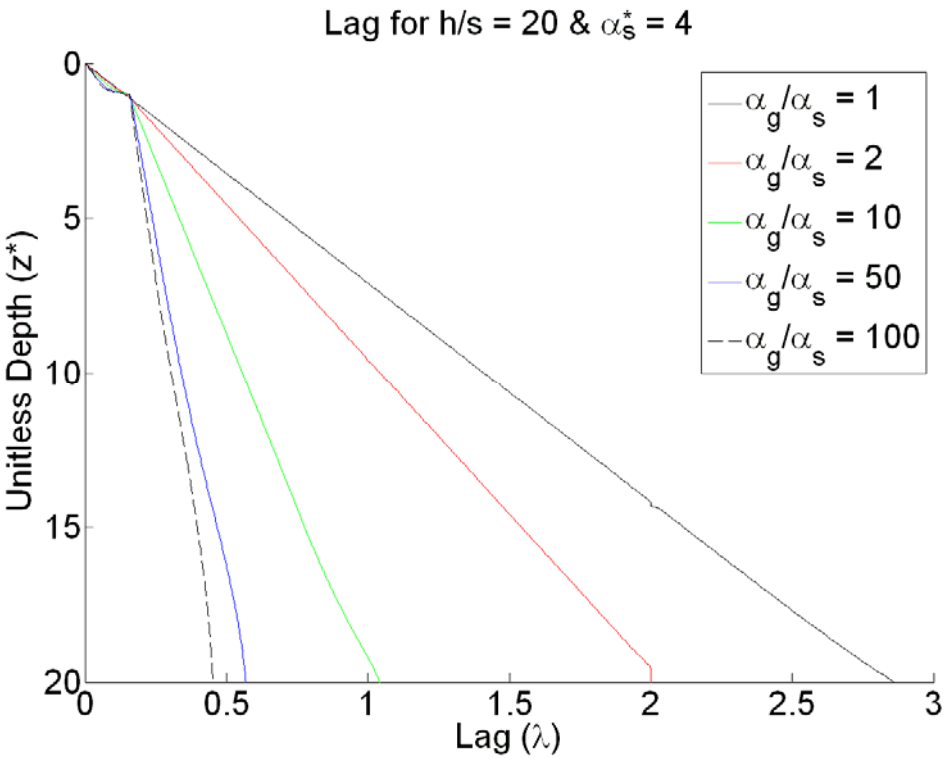

Figure 3.5b – Lag (λ) for α^*_s = 4.0

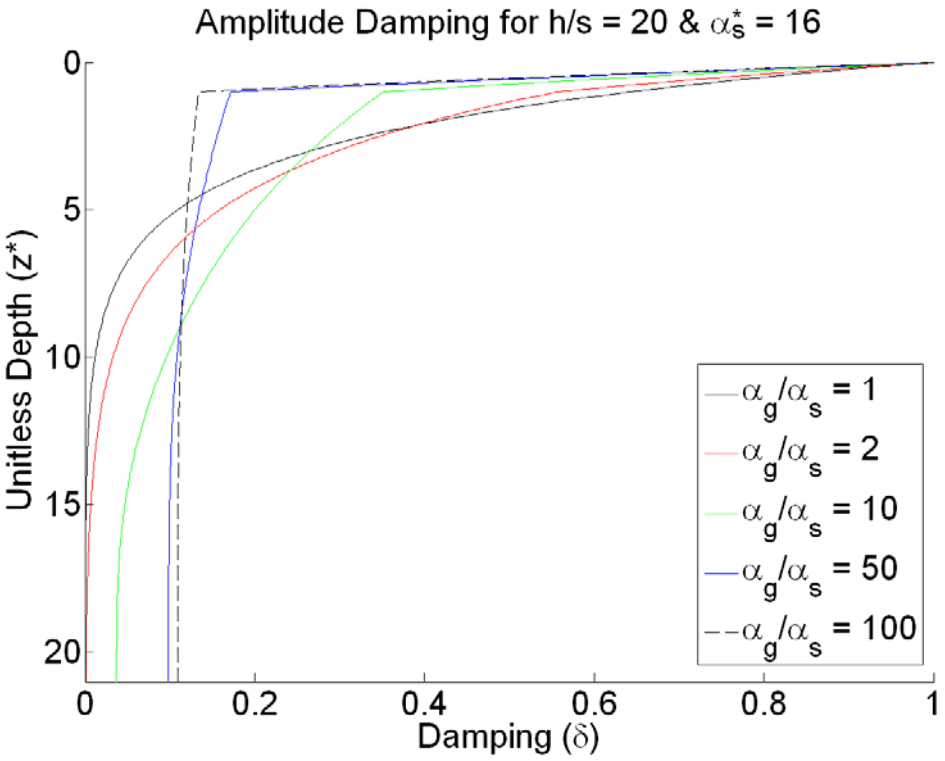

Figure 3.4c – Damping factor (δ) for α^*_s = 16.0 and *h/s* = 20

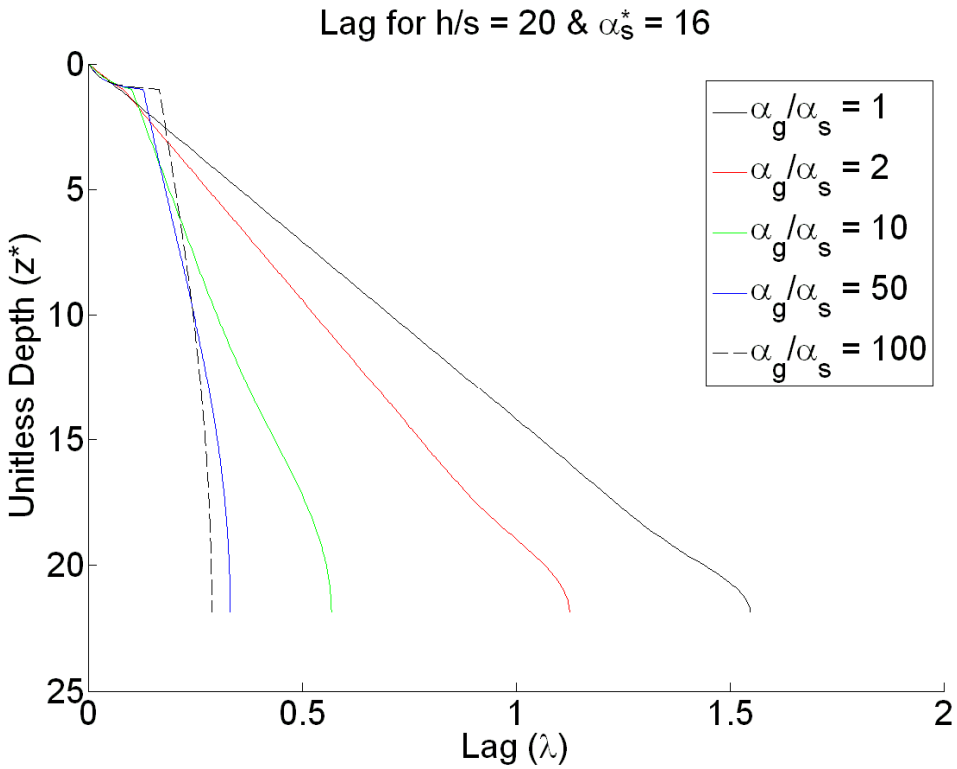

Figure 3.5c – Lag (λ) for α^*_s = 16.0

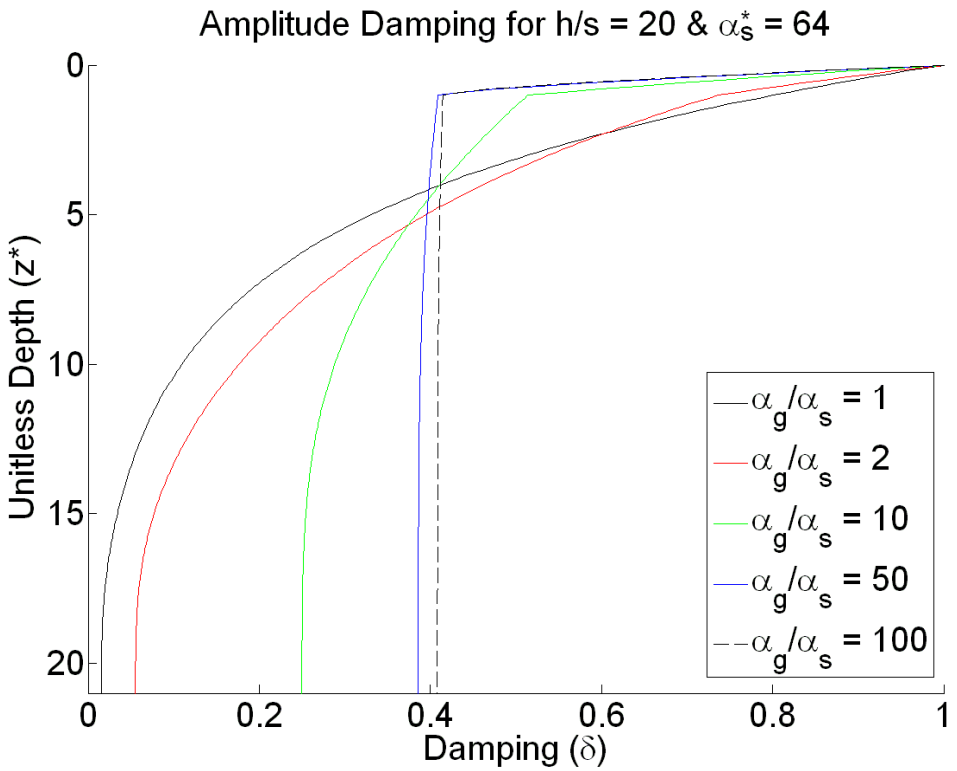

Figure 3.4d – Damping factor (δ) for α^*_s = 64.0 and *h/s* =20

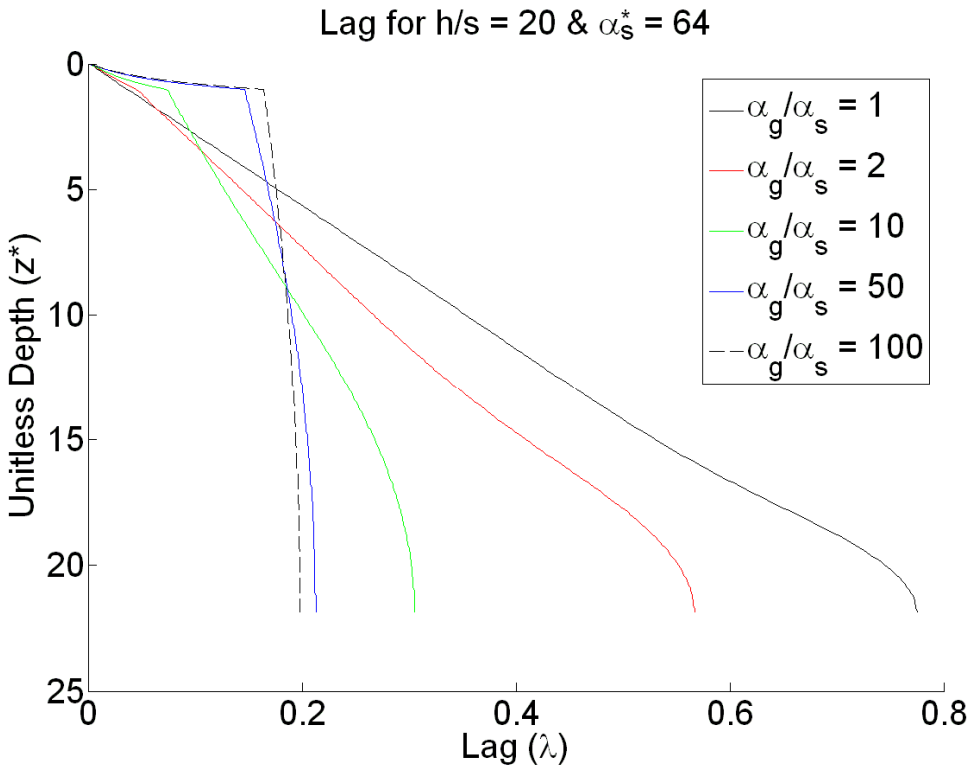

Figure 3.5d – Lag (λ) for α^*_s = 64.0

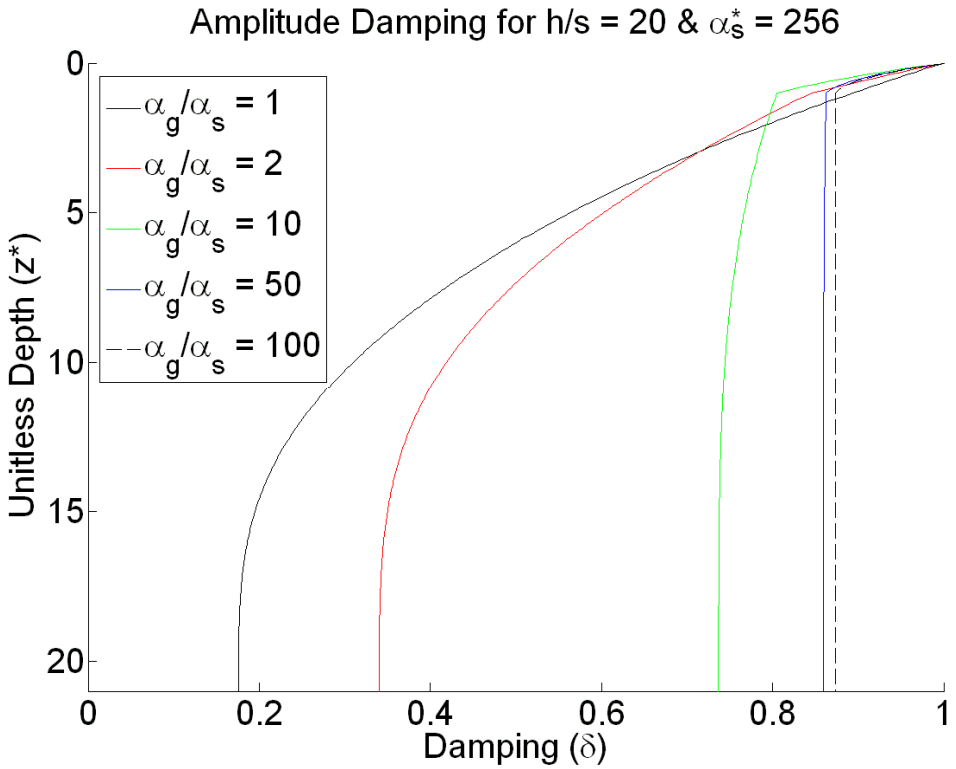

Figure 3.4e – Damping factor (δ) for α^*_s = 256.0 and *h/s* = 20

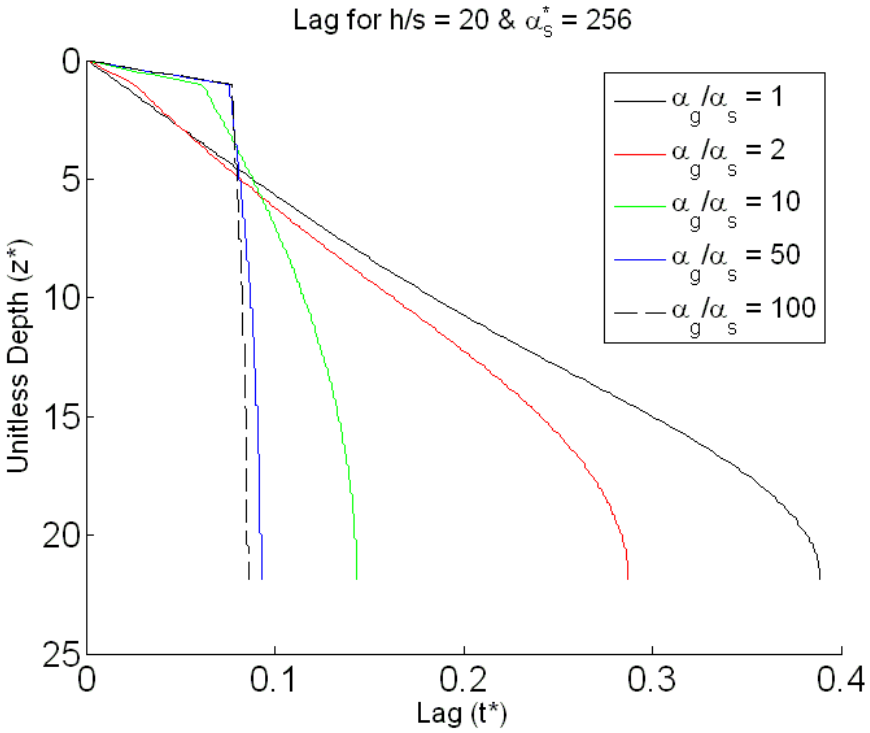

Figure 3.5e – Lag (λ) for α^*_s = 256.0 and *h/s* = 20

3.3 Estimation of year-round groundwater temperatures

This section contains a sample problem outlining the calculations associated with heat conduction from the surface into groundwater.

The first step is to determine the characteristics of site.

Annual Surface Temperature Data:

Mean temperature (T_m)= 10°C
Amplitude (ΔT) = 12.5°C
Period (t_0) = 365 days
Time of maximum temperature = 7/25 @1600 (day 207.67)

Aquifer Dimensions and Flow Properties

Depth to groundwater (S) = 1 m
Aquifer thickness (h) = 10 m
Groundwater velocity (V) = 0.75 m/day

Soil and Water Data (See Appendix A)

Soil type: 23-30 Ottawa Sand
Specific heat of the sand (c_p) = 766.18 J/kg/°C
Sand density (ρ) = 2650 kg/m^3
Mean grain size (d) = 0.73 mm
Heat capacity of sand (C_s) = 2030377 J/m^3/°C
Heat capacity of water (C_w) = 4186800 J/m^3/°C

Heat capacity of air (C_a) = 1256 J/m^3/°C
Porosity (n) = 0.35
Unsaturated moisture content ($M.C.$) = 5.5%

With the foregoing basic characteristics the saturated moisture content ($M.C._{sat}$) and percent saturation can be determined using equations (A.8) and (A.9), respectively.

$$M.C._{sat} = 100 * n\frac{\rho_w}{\rho} = 100 * 0.35\frac{1000}{2650} = 13.2\%$$

$$\%Saturation = 100\frac{M.C.}{M.C._{sat}} = 100\frac{5.5}{13.2} = 41.6\%$$

The thermal diffusivity of the unsaturated zone (α_s) needs to be calculated next. To do this the thermal conductivity (κ) can be determined using equation (A.5) and the heat capacity (C_1) can be determined using equation (A.3).

$$\kappa = 3844.05 * (0.7Log(M.C.) + 0.4)10^{(0.000624\rho)}$$
$$\cdots = 3844.05 * (0.7Log(5.5) + 0.4)10^{(0.000624*2650)} = 20{,}474\frac{J}{m \cdot day \cdot ^\circ C}$$

Equation (A.3) requires the volume fractions of solids, water, and air. The volume fraction of solids (V_s) can be determined from the porosity (n).

$$V_s = 1 - n = 1 - 0.35 = 0.65$$

The volume fraction of water (V_w) can be determined from the percent saturation and the porosity.

$$V_w = \frac{\%Saturation * n}{100} = \frac{41.6 * 0.35}{100} = 0.15$$

The volume fraction of air (V_a) can be determined from the volume fraction of solids and water.

$$V_a = 1 - V_s - V_w = 1 - 0.65 - 0.15 = 0.20$$

The heat capacity can now be calculated.

$$C_1 = V_s \cdot C_s + V_w \cdot C_w + V_a \cdot C_a$$
$$\cdots = 0.65 * 2030377 + 0.15 * 4186800 + 0.20 * 1256 = 1{,}930{,}000\frac{J}{m^3 \cdot ^\circ C}$$

De Vries (1966) notes that the air term can typically be omitted because it is so small. In this example the air term only equals 257 J m^{-3} °C^{-1}.

With the thermal conductivity and the heat capacity the unsaturated thermal diffusivity (α_s) can be determined using equation (A.1).

$$\alpha_s = \frac{\kappa}{\rho \cdot c_p} = \frac{\kappa}{C_1} = \frac{20{,}474}{1{,}930{,}000} = 0.0106 \frac{m^2}{day}$$

$$\alpha_s^* = \frac{\alpha_s \cdot t_0}{S} = \frac{0.0106 * 365}{1} = 3.87$$

The thermal diffusivity in the saturated soil (α_{sat}) can be calculated using the same method as for the unsaturated zone. For the saturated zone the following results are obtained:

κ = 66,584 J/m/day/°C
V_s = 0.65
V_w = 0.35
V_a = 0
C_2 = 2,785,000 J/m^3/°C
α_{sat} = 0.0239 m^2/day

The thermal diffusivity for the (saturated) aquifer needs to be corrected for hydrodynamic effects. Hydrodynamic dispersion depends on Peclet number (Pe), which can be calculated from equation (B.1).

$$Pe = \frac{V \cdot d}{\alpha_{sat}} = \frac{0.75 * 0.00073}{0.0239} = 22.9$$

Since the Peclet number is greater than five and less than 605 the longitudinal hydrodynamic dispersion can be calculated using equation (B.2).

$$\alpha_L = \alpha_{sat} * 0.5(Pe)^{1.2} = 0.0239 * 0.5(22.9)^{1.2} = 0.512 \frac{m^2}{day}$$

Since transverse hydrodynamic dispersion is assumed to be 1/3 of longitudinal hydrodynamic dispersion:

$$\alpha_g = \alpha_T = \frac{\alpha_L}{3} = \frac{0.512}{3} = 0.171 \frac{m^2}{day}$$

$$\alpha_g^* = \frac{\alpha_g \cdot t_0}{S} = \frac{0.171*365}{1} = 62.3$$

$$\frac{\alpha_g^*}{\alpha_s^*} = \frac{62.3}{3.87} = 16.1$$

With the above information the soil and water temperatures at any time and any location can be approximated using Figures 3.3b and 3.4b or by using the solution method discussed in section 3.1. Figures 3.5 and 3.6 provide temperature profiles and seasonal temperature cycles, respectively, for this example problem.

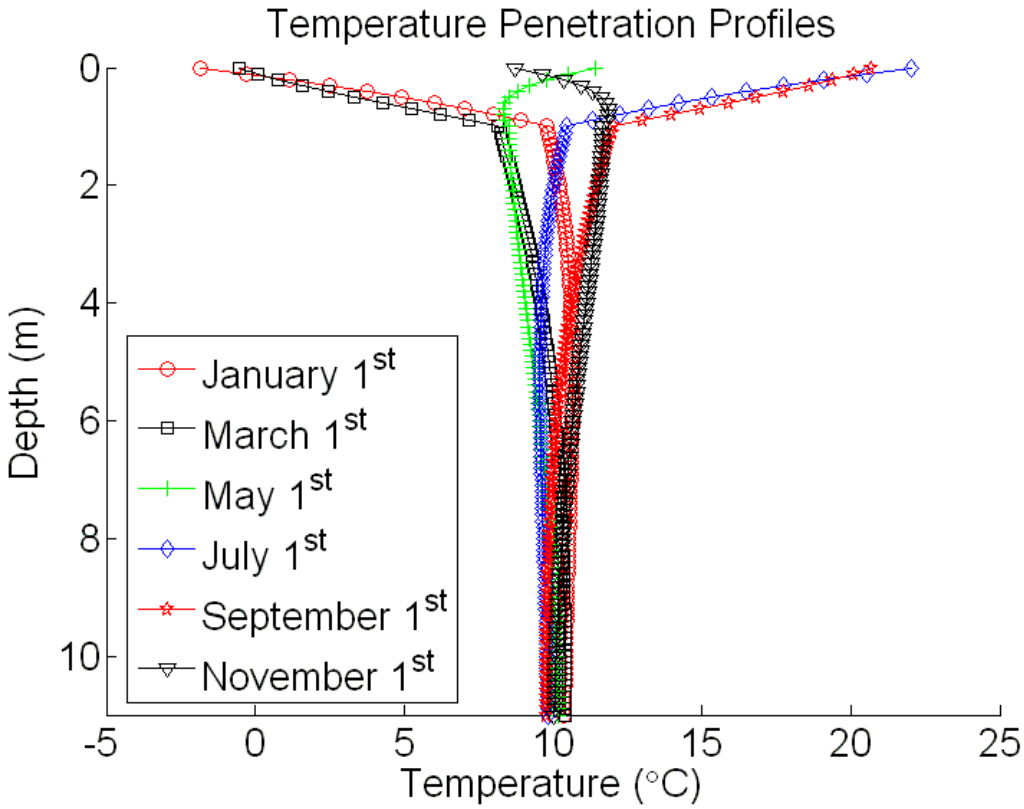

Figure 3.5 Temperature penetration profile for sample problem

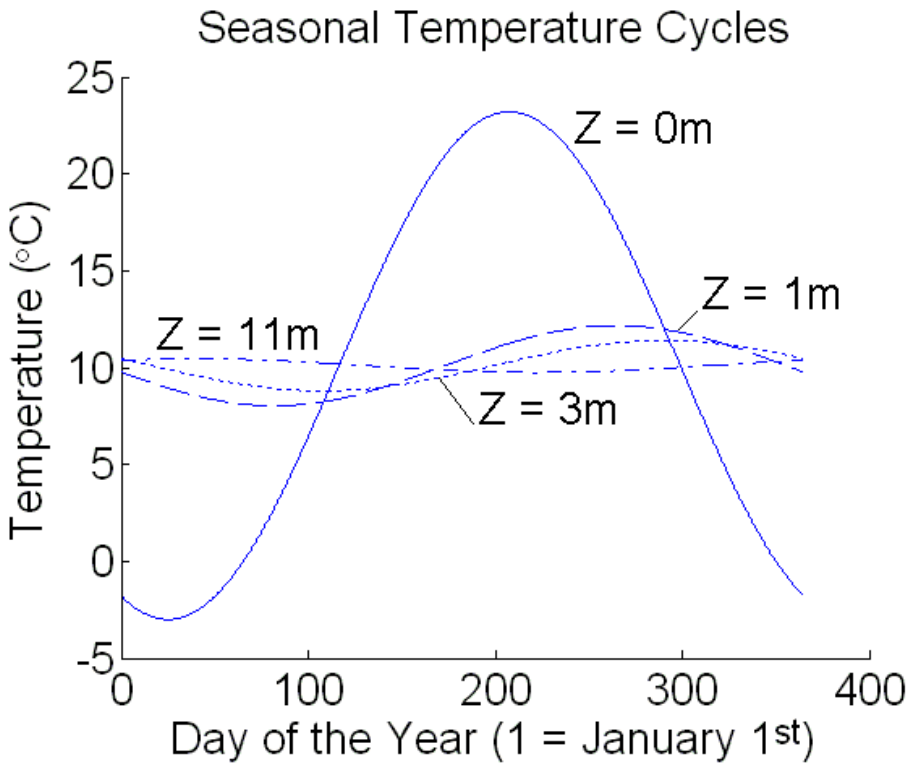

Figure 3.6 Seasonal temperature cycles for sample problem

4. Field measurements

In groundwater temperature modeling studies the lack of monitoring data for model validation is often a problem. In many analyses the lack of data has made it difficult to verify simulated groundwater temperatures. Appendix D provides a short explanation of groundwater monitoring schemes that would be beneficial. The Minnesota Pollution Control Agency (MPCA) has, however, collected groundwater data in the St. Cloud area from spring 1997 to spring 2001 to determine the effect of land use on groundwater quality (Figure 4.1), including concentrations of metals and chemical species, suspended solids and temperature (MPCA 2001). These data indicate that the average groundwater temperature recorded below residential and commercial properties is warmer than below agricultural and undeveloped properties. These findings are consistent with Herb et al.'s (2007) surface temperature simulation results, because residential and commercial properties usually have buildings and paved surfaces that are kept at an elevated average temperature year-round by solar or artificial heating while agricultural and undeveloped land receives less net heat input.

The MPCA's analysis was concerned primarily with chemical contaminants and did not consider the depth of the wells or the time of the year when comparing groundwater temperatures. We have re-evaluated the MPCA's St. Cloud groundwater monitoring data to determine groundwater temperature

dependence on ground surface temperature, depth from the ground surface, and time of year. The St. Cloud data were divided according to land use and well depth. Data from domestic wells were omitted from the data set because well pumping draws water from uncertain depths above and below the well screen. The monitoring well data fell into 18 categories arranged by land use and sampling depth.

Table 4.1 Seasonal temperature characteristics of groundwater in the St. Cloud, MN, area (MPCA 2001)

Land Use	Depth (ft)	T_m (°C)	ΔT_f (°C)	Fitted Phase Shift ( )	Fitted Phase Shift (day)	RMS Error (°C)
commercial/industrial	11	10.7	6.2	0.347	126.824	1.44
commercial/industrial	16.5	10.2	3.5	0.309	112.691	1.07
commercial/industrial	18.5	12.6	2.7	0.228	83.129	1.14
irrigated agriculture	17.2	9.6	2.7	0.273	99.691	1.18
irrigated agriculture	25	10.0	0.8	0.332	121.113	0.36
nonirrigated agriculture	10	10.7	2.7	0.330	120.541	1.05
nonirrigated agriculture	12.5	9.9	6.7	0.276	100.870	0.71
nonirrigated agriculture	16.2	8.6	2.4	0.387	141.248	1.84
nonsewered residential	17.4	11.1	2.6	0.260	94.791	0.92
nonsewered residential	22	12.2	1.1	0.292	106.647	0.64
nonsewered residential	24.5	12.5	1.7	0.300	109.343	1.70
sewered residential	20	10.5	1.6	0.151	54.945	0.20
sewered residential	22	11.3	1.5	0.224	81.774	0.62
sewered residential	31	11.1	1.2	0.373	136.218	0.59
undeveloped	10	10.4	3.2	0.306	111.776	1.67
undeveloped	12	9.0	3.3	0.347	126.767	0.75
undeveloped	13	10.7	2.4	0.267	97.374	0.60
undeveloped	45	9.0	1.4	0.436	159.027	0.55

Equation (2.8) was fitted to each of the data sub-sets to determine the mean annual temperature, the fitted seasonal amplitude, and the fitted phase shift. According to the theory summarized in Sections 2 and 3 the mean temperature in the groundwater and the mean temperature at the groundwater surface should be the same. Results of the analysis indicate that the average groundwater temperature below commercial and residential properties in the St. Cloud area is 11.4°C (standard deviation = 0.88°C), while the average temperature below agricultural and undeveloped land is 9.8°C (standard deviation = 0.77°C). This agrees with the MPCA (2001) analysis, and with Herb et al.'s (2007) results. A summary of the results obtained by fitting Equ.(2.8) to the St. Cloud data is given in Table 4.1.

The direction and velocity of the groundwater flow around a monitoring well can influence the results. If the groundwater near a given monitoring well is flowing fast, it is conceivable that the groundwater temperature observed in a well is affected by the surface temperatures of adjacent land use types.

The most distant location of a potentially influential surface heat source can be estimated by first determining the time required for heat to penetrate from the groundwater table to the monitoring depth. The heat penetration time (t_p) is the lag time (Equ. 4.1).

$$t_p = t_0 \cdot \lambda(z) \tag{4.1}$$

where $\lambda(z)$ = dimensionless lag
t_0 = seasonal period = 365 days

The penetration time (t_p) can be multiplied by the maximum groundwater velocity to determine the maximum distance to a surface heat source for a given well. For the purposes of establishing a well capture zone, the maximum groundwater velocity was estimated using Darcy's Law

$$u = \frac{k}{n}\frac{d\phi}{dx} \tag{4.2}$$

where k = hydraulic conductivity
$d\phi/dx$ = hydraulic gradient

MPCA (2001) conducted several pumping tests throughout the St. Cloud area, and the greatest recorded hydraulic conductivity was reported as k = 0.001724 cm/s (1.51 m/day). According to Figure 4.1 the maximum hydraulic gradient near the monitoring wells is $d\phi/dx$ = 20 ft/ 0.5 miles (0.0076 m/m). Using these values and equation (4.2) the maximum groundwater velocity is estimated to be 0.04 m/day. With a groundwater velocity this slow, it is to be expected that the observed groundwater temperatures are impacted only by the land use immediately around the well.

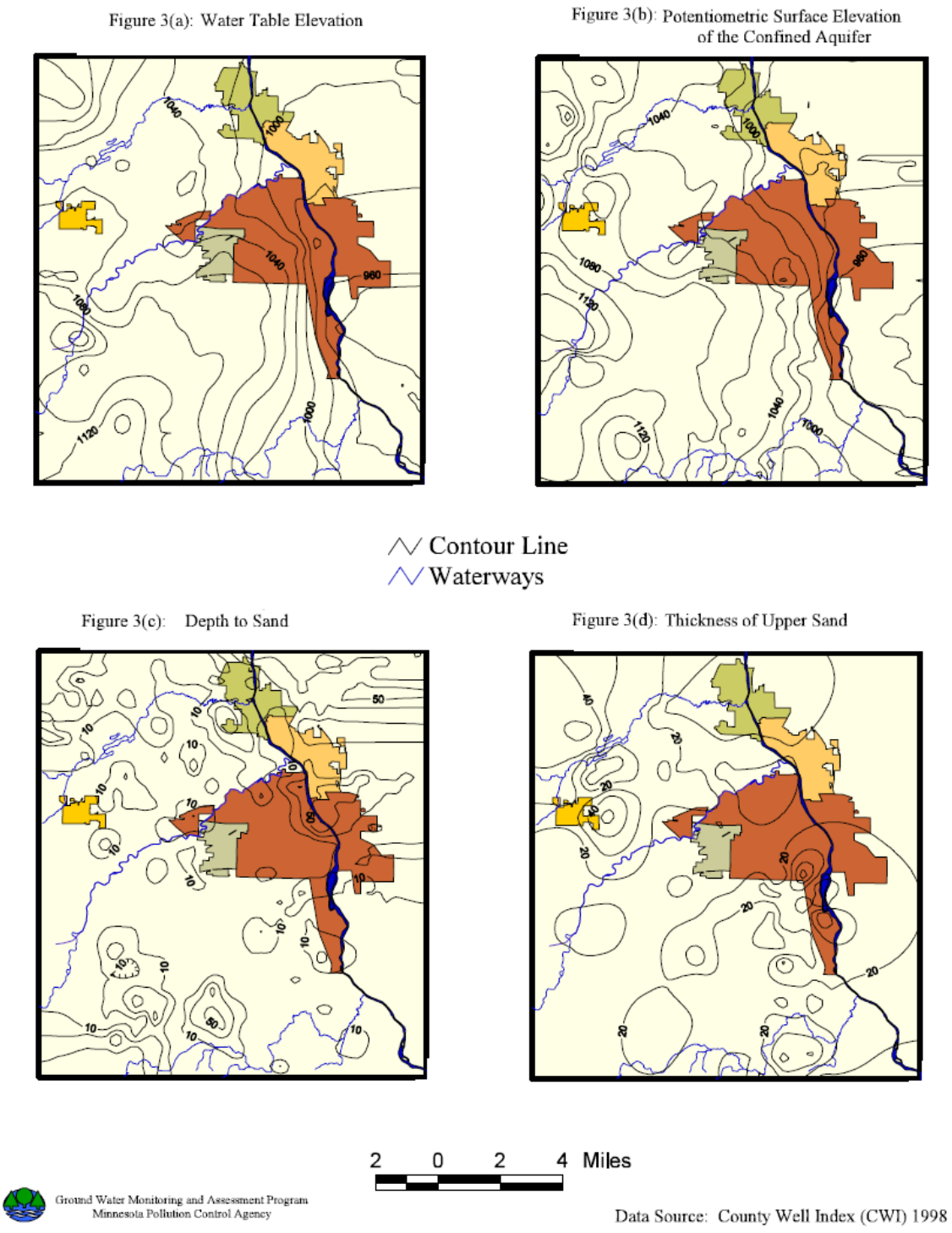

Figure 4.1 Hydrogeologic maps of the St. Cloud shallow (quaternary) aquifer (from MPCA 2001)

5. Projections of the effect of urban development on vertical heat conduction into the ground and resulting shallow groundwater temperatures

5.1 Urbanization effects on shallow aquifer temperatures

The relationships developed in the previous sections can be used to estimate by how much shallow groundwater temperatures may change when agricultural or natural land is converted to urban development. Figures 2.2, 2.7, 2.8, and 3.6 demonstrate that the mean annual temperatures of the soil and the groundwater below it are the same as the mean annual temperature as the ground surface. Surface cover type affects the ground surface temperature strongly (Figure 1.1), and, hence, the temperatures below the surface. Asphalt and concrete surfaces reach higher surface temperatures at daytime under clear sky (high solar radiation) than surfaces with plant cover, while night temperatures of most ground surfaces are more comparable (Herb et al. 2006). Grass provides enough shade to maintain surface temperatures similar to agricultural or undeveloped land. As a result asphalt and concrete surfaces have higher mean temperatures (T_m) and larger seasonal temperature amplitudes (ΔT) than surfaces with vegetation covers.

Mean annual temperatures and seasonal amplitudes of the soil near the ground surface are given in Table 5.1.The temperatures at 1cm to 1in depth into the soil below the surface are used because the temperature at the surface itself (air/soil boundary) can fluctuate rapidly due to weather conditions. The values given in Table 5.1 were derived by fitting seasonal cycles (Equ. 2.8) to data from the St. Paul, MN, site for grass cover and bare soil and the MnROAD site near Albertville, MN, for asphalt and concrete surfaces. At both sites six years of data were used to fit the seasonal cycles. Plots of these typical surface temperatures are included in Figure 5.1. Diurnal cycles of ground surface temperatures are not included in Table 5.1 or in Figure 5.1.

Table 5.1 Mean annual ground surface temperatures and seasonal amplitudes near the Twin Cities, Minnesota

Surface Type	T_m (°C)	ΔT (°C)	T_{max} (°C)	T_{min} (°C)	Source
Sod	10.1	13.06	23.16	-2.96	St. Paul Site
Bare Soil	10.39	15.28	25.67	-4.89	St. Paul Site
Asphalt	13.22	18.6	31.82	-5.38	MnROAD
Concrete	11.83	16.43	28.26	-4.6	MnROAD
Building	23.2	8.6	31.8	14.6	DOE/EPA

For surfaces covered by buildings, the temperature inside the building can be used as the surface temperature. A building's roof temperature is not a reasonable approximation for the temperature below the building. The interior temperatures are controlled or influenced by activities inside, the building. The maximum and minimum building temperatures used in Table 5.1 are based on the US Environmental Protection Agency's and the US Department of Energy's "Energy Star" home recommendations (USEPA and USDOE).

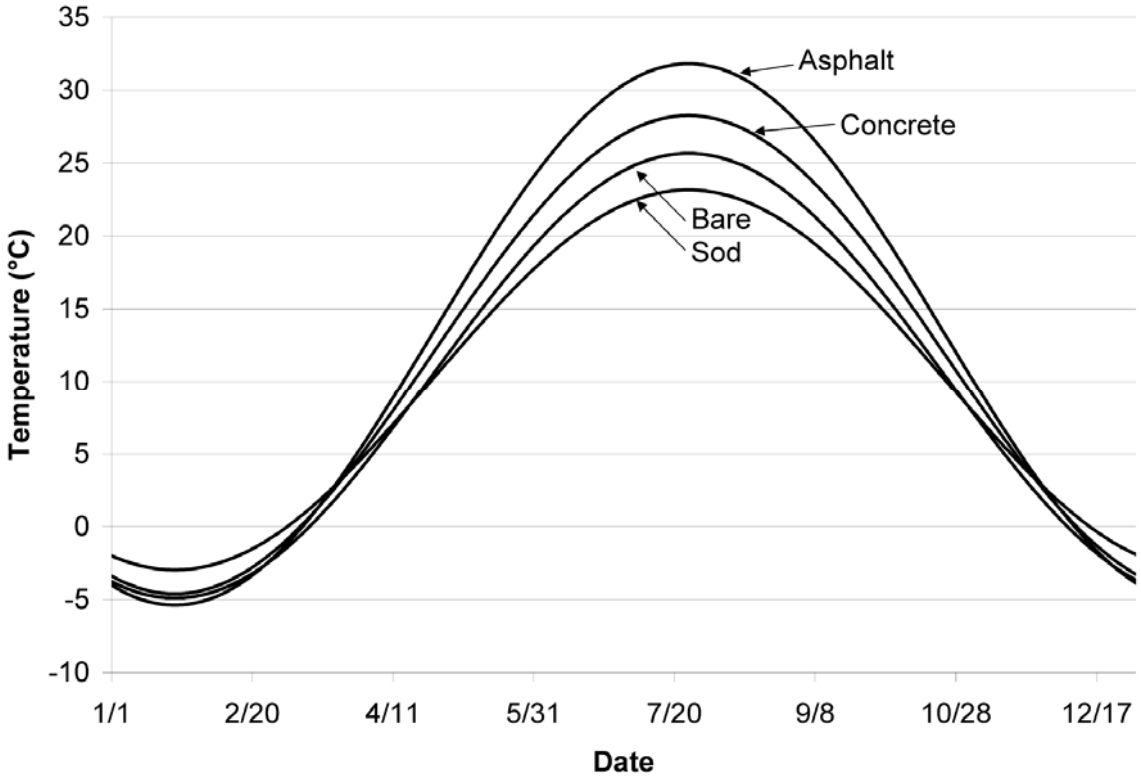

Figure 5.1 – Typical seasonal temperature cycles of asphalt, concrete, sod, and bare soil in/near the Twin Cities Metropolitan Area.

Buildings, asphalt and concrete have higher mean annual surface temperatures than grass and bare soil (Table 5.1). Urbanization can therefore be expected to raise ground surface temperatures of the composite urban landscape by a noticeable amount. In addition, and not related to seasonal ground temperature cycles, daily maximum and minimum surface temperatures in summer differ on average by 25-30^{o}C for asphalt and concrete surfaces, by 15 to 20^{o}C for roof tops, but only by 2^{o}C under grassland.(Herb et al. 2007).

According to equation (2.7) and the definition of dimensionless temperature (T^{*}), the mean annual ground temperature and the mean annual shallow groundwater temperatures have to change by the same amount as the mean ground surface temperature.

The seasonal temperature amplitude of shallow urban groundwater will increase if the ground surface temperature amplitude increases (Section 3). Setting the regional mean surface temperature equal to the regional mean groundwater temperature implies that the soils over a region have a horizontally homogeneous density and specific heat. This is a reasonable assumption, in most cases, because the soil properties tend to vary much more vertically than horizontally.

The mean surface temperature of any region depends on the surface types that make up that region. For example, agricultural areas in Japan are expected to have the following surface type distribution (Paringit and Nadaoka 2003): crops 96%, bare soil 1%, and structures 3%. Urban surface type distributions in the United States have been measured for various land uses in several cities: Sacramento, California (Akbari et. al 1999), Salt Lake City, Utah (Akbari and Rose. 2001a), Chicago, Illinois (Akbari and Rose. 2001b), and Houston, Texas (Rose et. al. 2003). Table 5.2 gives averages of the surface types in these four cities.

Table 5.2 Surface types (%) for different urban land uses in four U,S. Cities

Land Use	USGS LULC	% Tree	% Roof	% Road	% Sidewalk	% Parking	% Barren	% Grass	% Misc.
Residential	11	15.7	21.4	13.0	7.2	5.1	4.8	29.1	3.8
Commercial/Service	12	7.4	22.1	15.0	2.9	30.5	5.9	12.3	3.9
Industrial	13	4.4	23.2	8.6	0.8	22.5	15.6	16.1	9.0
Transportation/Communications	14	0.5	8.6	48.3	0.3	16.1	4.6	6.0	15.5
Industrial and Commercial	15	3.8	23.4	11.0	1.4	29.0	9.9	14.3	7.4
Mixed Urban or Built-up Land	16	14.6	23.7	15.4	3.3	15.0	3.7	19.1	5.4
Other Mixed Urban or Built-up Land	17	13.4	22.5	10.4	2.7	18.6	10.0	16.2	6.2

USGS LULC = The US Geological Survey land use/land cover classification

If surface temperatures from Table 5.1 are assigned to each surface type in Table 5.2 the expected composite (area-weighted) surface temperatures for each land use can be determined (Table 5.3). It is assumed that roads and parking areas have asphalt pavements, sidewalks are concrete, and trees and grass have the same surface temperatures. The expected surface temperature for each land use type is determined by taking the weighted average of the individual surface temperatures for each of the surface types. Averaging the maximum and minimum temperatures is made with the assumption that these two temperatures occur at the same time for each surface type.

Table 5.3 Expected composite (annual) surface temperatures for different urban land uses in four U.S. Cities from Table 5.2

Land Use	USGS LULC	Weight Avg Temperature (°C)	Weight Max Temperature (°C)	Weight Min Temperature (°C)
Agricultural		10.4	23.3	-2.4
Residential	11	13.7	27.2	0.3
Commercial/Service	12	14.7	29.6	-0.2
Industrial	13	14.6	28.8	0.3
Transportation/Communications	14	13.8	30.8	-3.1
Industrial and Commercial	15	14.8	29.4	0.2
Mixed Urban or Built-up Land	16	14.5	28.4	0.5
Other Mixed Urban or Built-up Land	17	14.3	28.3	0.3

Erickson (2008) estimated the past, current, and projected land uses in a region with extensive urban development near Lakeville, Minnesota. The land use distributions reflect different urbanization scenarios. Erickson's land use types are slightly different from the land use types in Tables 5.1 and 5.2. Table 5.4 is an adaptation of Erickson's (2008) urbanization (land use) scenarios. Table 5.5 gives the expected average ground surface temperatures for Lakeville, Minnesota under current climate conditions for the land use scenarios presented in Table 5.4.

Table 5.4 Land use distributions for different urban development scenarios in Lakeville, Minnesota (Erickson 2008)

Land Use	Pre-Development	Present	Plus 50 yr	Plus 100 yr
Agricultural	85%	59%	45%	29%
Residential	12%	29%	42%	56%
Commercial/Service	3%	10%	11%	13%
Industrial	0%	1%	1%	1%
Transportation/Communications	0%	1%	1%	1%

Table 5.5 Expected composite (annual) ground surface temperatures for urban land development scenarios in Lakeville, Minnesota from Table 5.4

	Pre-Development	Present	Plus 50 yr	Plus 100 yr
Maximum Temperature (°C)	24.0	25.2	25.8	26.5
Mean Temperature (°C)	11.0	11.9	12.4	12.9
Minimum Temperature (°C)	-2.1	-1.4	-1.0	-0.6

The 100 year land use projection still contains some agricultural areas and does not represent the full development to a 100% urban area. Using the fully urbanized surface type distribution for the Chicago downtown area (Akbari and

Rose 2001b), the expected average (annual) ground surface temperatures are: maximum temperature = 27.1°C, mean temperature = 13.9°C, and minimum temperature = 0.6°C.

Figure 5.2 gives a graphical view of the annual ground surface temperatures under various urbanization scenarios at the finges of the Twin Citries Metropolitan Area (TCMA) (Table 5.5). Figure 5.2 suggests that each step of urbanization results in a stepwise increase in ground surface and consequently shallow groundwater temperatures.

According to Table 5.5 the full development of an agricultural area to a fully urban area at the fringes of the Twin Cities Metropolitan Area (TCMA) is expected to result in a 2.9°C mean annual ground surface temperature increase, and consequently a 2.9°C increase in the mean annual temperature of shallow groundwater. The maximum seasonal average surface temperature may rise by 3.1°C, and the minimum by 2.7°C.

Groundwater provides the base flow to many cold-water streams. A 1.9°C rise in base flow water temperature could potentially be devastating to coldwater fish inhabiting the stream.

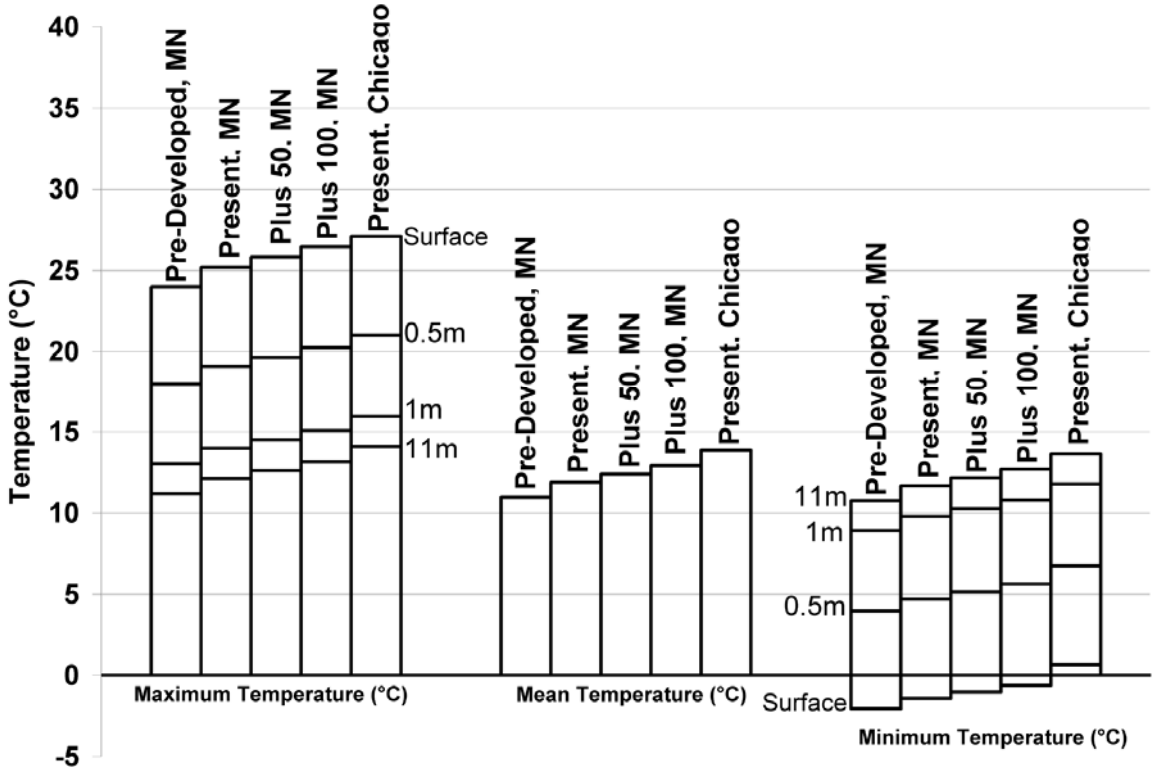

Figure 5.2 – Expected sub-surface temperatures due to various degrees of urbanization scenarios using soil and aquifer properties from the example in Section 3.3 (Groundwater depth (S) = 1.0m)

5.2 Urbanization effects on deep aquifer temperatures

Section 2.1 showed that the seasonal (annual) amplitude of the ground surface temperature decays exponentially with depth. For aquifers with groundwater tables deeper than about 12m below the ground surface, seasonal temperature fluctuations that reach the water table are so small that they can be ignored; however, mean annual temperatures of deep aquifers can be expected to rise by the same amount as mean annual ground surface temperatures when an agricultural or natural area is replaced by urban development.

6. Projections of global climate change effects on temperatures of shallow and deep groundwater

Global climate warming has been documented by the IPCC (2007). Its causes are still being debated. Under most climate change scenarios, the mean annual air temperature is projected to increase. For a continuing rise in atmospheric CO_2, the IPPC (2007) has assembled projected air temperature rises between 1.1 and 6.4°C with an average around 2.8°C by 2100 (Table 6.1).

Table 6.1 Projected globally averaged surface warming at the end of the 21st century for different model cases (Table SPM-2 from IPCC 2007). Air temperature Change (°C) in 2090-2099 relative to 1980-1999)

Case	Best Estimate	Likely Range
B1 scenario	1.8	1.1 – 2.9
A1T scenario	2.4	1.4 – 3.8
B2 scenario	2.4	1.4 – 3.8
A1B scenario	2.8	1.7 – 4.4
A2 scenario	3.4	2.0 – 5.4
A1FI scenario	4	2.4 – 6.4

The mean ground surface temperature used in our analysis of shallow groundwater temperatures depends on more than air temperature. The ground surface temperature is the temperature at which the sum of all heat fluxes received or emitted by the ground surface is zero. Ground surface temperatures are calculated based on this heat balance (Herb et al. 2006). To obtain the projected ground surface temperatures during climate change the heat flux balance has to be recalculated for future climate scenarios.

If all radiative and evaporative heat fluxes were to remain the same, then the convective heat flux, which is related to air temperature, would be the only factor that would change ground surface temperatures. In that unlikely case, the mean annual groundwater temperature rise would equal the projected mean annual air temperature rise in Table 6.1.

To obtain projected ground surface temperatures (NOT air temperatures) we selected a projected $2xCO_2$ climate scenario which was previously used for lake and stream water temperature projections (Fang and Stefan, 2004). The new climate data were obtained by applying mean monthly increments or ratios to recorded weather data. The monthly increments or ratios represent the differences between a $1xCO_2$ and a $2xCO_2$ climate scenario as simulated by the atmospheric General Circulation Model (GCM) of the Canadian Climate Center (CCC). The increments or ratios used are listed in Table 6.2.

Table 6.2 Increments and ratios for climate parameters to be applied to historical weather data time series in order to obtain the $2xCO_2$ climate scenario weather data (Values obtained from the Canadian Climate Center General Circulation Model, CCCGCM (Boer et al. 1992, see Fang and Stefan, 2004).

Month	Air temperature (°C)[a]	Solar radiation ratio[b]	Wind speed ratio[b]	Specific humidity ratio[b]	Precipitation ratio[b]
Jan	8.17	0.94	1.08	1.85	1.23
Feb	8.50	0.92	1.10	1.94	1.26
Mar	4.37	0.95	0.88	1.53	1.22
Apr	5.76	0.95	1.01	1.78	1.50
May	5.39	0.97	0.97	1.46	1.05
Jun	4.27	0.96	0.85	1.32	0.99
Jul	3.54	0.96	0.80	1.23	0.87
Aug	5.24	0.99	0.83	1.35	0.87
Sep	4.51	0.99	0.90	1.29	0.79
Oct	2.71	0.98	1.01	1.19	0.96
Nov	2.9	1.01	1.02	1.29	0.96
Dec	4.38	1.00	0.91	1.25	0.97

[a] Increment = 2xCO2 CCC GCM output – 1xCO2 CCC GCM output
[b] Ratio = 2xCO2 CCC GCM output divided by 1xCO2 CCC GCM output

One can see in Table 6.2 that in summer solar irradiance is diminished, humidity is increased and wind speed is reduced. The first two are the result of a higher atmospheric moisture content. The qualitative result of these changes

would be less heating of a ground surface by solar radiation and less cooling by evapotranspiration. The net result cannot be guessed.

For the projected $2xCO_2$ climate scenario we recalculated the ground surface heat balance using the model by Herb et al. (2006) and obtained new ground surface temperatures. The recalculated ground surface temperature was higher than those given in Table 5.1 and Figure 5.1. The monthly differences between ground surface temperatures under the 2xCO2 scenario and the 1xCO2 scenario were calculated and are shown in Figure 6.1. The temperature increments from Figure 6.1 were applied to the ground surface temperature data used to develop Table 5.1, and the projected mean annual ground surface temperatures and seasonal amplitudes for a 2xCO2 climate scenario were determined by fitting a seasonal cycle (Equ. 2.8) to the data. Table 6.3 provides the results of the seasonal cycle fittings for each of the surface types. In all cases, with the exception of the building surface type, the projected annual mean temperatures increased from the current typical mean temperatures. The projected seasonal amplitudes, however, did not change by much. This means that the projected maximum and the projected minimum temperatures both increased by about the same increment as the projected annual mean temperature.

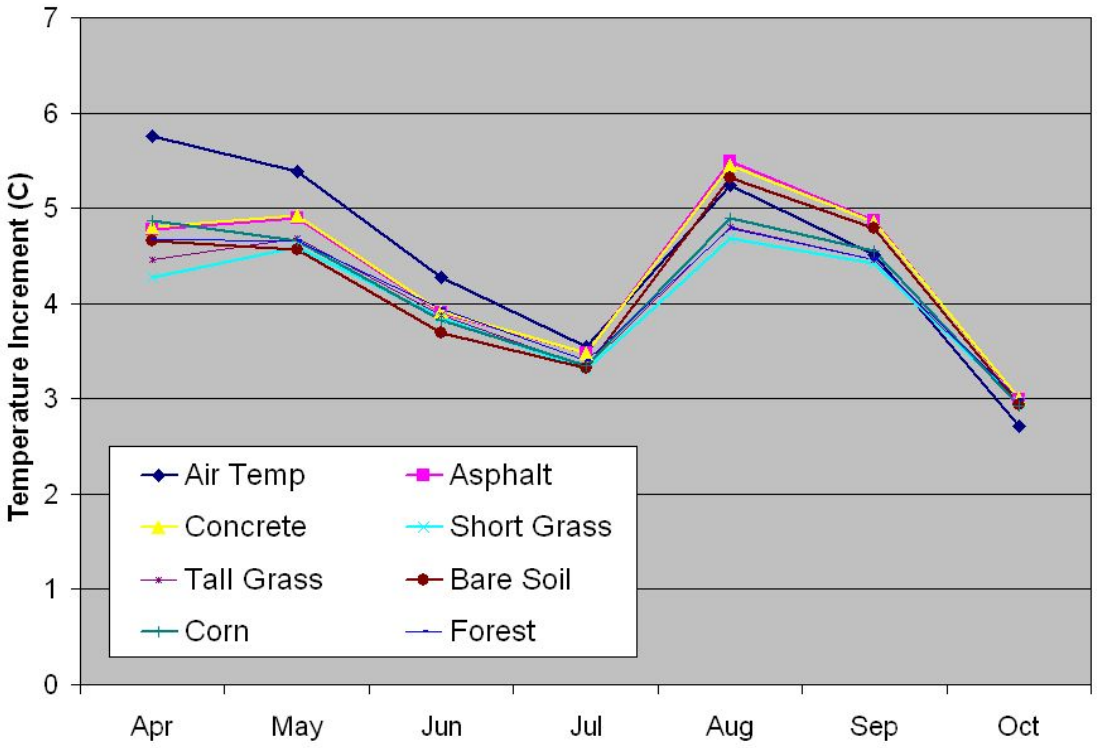

Figure 6.1 – Projected ground surface temperature increments for the 2xCO2 scenario climate scenario calculated by the Herb et al. (2006) method

Table 6.3 Projected annual ground surface temperatures and seasonal amplitudes under a 2xCO_2 climate scenario

Surface Type	T_m (°C)	ΔT (°C)	T_{max} (°C)	T_{min} (°C)	L
Sod	12.91	14.9	27.81	-1.99	0.36
Bare Soil	10.39	15.28	25.67	-4.89	0.38
Asphalt	17.65	18.46	36.11	-0.81	0.38
Concrete	16.34	16.5	32.84	-0.16	0.36
Building	23.2	8.6	31.8	14.6	

A 2xCO_2 climate scenario is a fairly extreme projection. This pessimistic projection would, of course, be softened if the annual global CO_2 emissions were curbed. One can note that the average annual ground surface temperature rise projected for a 2xCO2 climate scenario in Figure 6.1 is on the order of 4.0°C, equal to the 4.0°C air temperature rise projected by the IPCC by the A1F1 scenario in Table 6.1. It is noteworthy that both projections are for a pessimistic emission scenario and for about the turn of the next century (2100). For a more optimistic projection of ground surface temperatures it may be legitimate to draw on the values given in Table 5.1 for air temperatures.

By applying the projected annual ground surface temperature results from Table 6.3 to the surface type breakdown for different land uses in Table 5.2 the projected ground surface temperatures by land use can be determined for the 2xCO_2 scenario (Table 6.4). Table 6.5, containing the temperature changes between Table 6.4 and Table 5.3, shows that, for all land uses included in this study, the 2xCO_2 scenario will cause an in increase in the mean, maximum, and minimum seasonal temperatures at a ground surface.

Table 6.4 Projected composite (annual) surface temperatures for different urban land uses under a 2xCO_2 climate scenario

Land Use	USGS LULC	Weight Avg Temperature (°C)	Weight Max Temperature (°C)	Weight Min Temperature (°C)
Agricultural		13.1	27.8	-1.5
Residential	11	16.2	30.5	1.9
Commercial/Service	12	17.5	32.7	2.3
Industrial	13	16.7	31.3	2.2
Transportation/Communications	14	17.4	34.4	0.4
Industrial and Commercial	15	17.3	32.2	2.4
Mixed Urban or Built-up Land	16	17.0	31.6	2.5
Other Mixed Urban or Built-up Land	17	16.7	31.3	2.1

Table 6.5 Projected increases in ground surface temperatures (annual mean, mean annual maximum, and mean annual minimum temperature) for different land uses in Lakeville, Minnesota under a 2xCO_2 climate scenario

Land Use	USGS LULC	Increase of Mean Temperature (°C)	Increase of Max Temperature (°C)	Increase of Min Temperature (°C)
Agricultural		2.7	4.5	0.9
Residential	11	2.5	3.3	1.6
Commercial/Service	12	2.8	3.1	2.5
Industrial	13	2.2	2.5	1.8
Transportation/Communications	14	3.6	3.6	3.6
Industrial and Commercial	15	2.5	2.8	2.2
Mixed Urban or Built-up Land	16	2.6	3.2	2.0
Other Mixed Urban or Built-up Land	17	2.4	2.9	1.8

7. Cumulative effects of urban development and global climate change on temperatures of shallow and deep groundwater in the Twin Cities Metropolitan Area of Minnesota

A cumulative increase in shallow groundwater temperatures due to urban development plus global climate change can occur. Urbanization and climate change occur gradually over many years. The resulting soil/groundwater temperature change can be expected to be more or less synchronized (quasi-steady state) with the progression of urbanization and climate change. By applying the projected ground surface temperature results for various land uses (Table 6.4) to the urban land development scenarios from Table 5.4, the effects of urbanization under a 2xCO_2 climate scenario can be assessed. Table 7.1 indicates that, like the current climate condition, urbanization under the 2xCO_2 climate scenario will cause a rise in the annual mean, annual maximum, and the annual minimum ground surface temperature. The groundwater temperatures will change by the same increments as the ground surface temperatures as discussed previously.

Table 7.1 Projected composite (annual) ground surface temperatures for urban land development scenarios in Lakeville, Minnesota, from Table 5.4 under the 2xCO_2 climate scenario

	Pre-Development	Present	Plus 50 yr	Plus 100 yr
Maximum Temperature (°C)	28.3	29.2	29.6	30.1
Mean Temperature (°C)	13.6	14.5	15.0	15.5
Minimum Temperature (°C)	-1.0	-0.1	0.4	1.0

Using pre-development (agricultural) land surface conditions and 2004 climate conditions as a reference, the incremental ground surface temperature changes for different levels of urban development under a 2xCO2 climate

scenario can be summarized as shown in Table 7.2. The values in Table 7.2. were obtained by subtracting the values in Table 5.5 from the values in Table 7.1.

Table 7.2 Projected increments in groundwater temperatures due to three levels of urban development (Plus 100 years = full urban residential and commercial development) and global climate change from 2004 to 2xCO_2

	Pre-Development	Present	Plus 50 yr	Plus 100 yr
Maximum Temperature (°C)	4.3	4.0	3.8	3.6
Mean Temperature (°C)	2.7	2.6	2.6	2.6
Minimum Temperature (°C)	1.1	1.3	1.4	1.6

Under the 2xCO2 scenario, the expected average (annual) ground surface temperatures for a degree of urbanization similar to the Chicago downtown area are: mean maximum annual temperature = 29.9°C, mean annual temperature = 16.2°C, and mean minimum annual temperature = 2.5°C. Combining the effects of urbanization and climate change in the extreme, the full development of an agricultural area into downtown area such as Chicago and applying the 2xCO_2 scenario will increase the mean annual surface temperature by 5°C. The mean annual groundwater temperatures would consequently be projected to increase by the same amount.

8. Summary and Conclusions

Groundwater is the primary source of water for many coldwater streams. Groundwater temperature is related to climate. Mean annual groundwater temperature is often equal to mean annual air temperature plus 1-3 ^{o}C. This is because groundwater gains or looses heat by conduction/convection from the ground surface temperature. We have analyzed this relationship in detail.

The mean annual ground surface temperature depends on land use and climate. The mean annual temperature of the ground surface and the mean annual temperature of the groundwater are often the same. Changes in land use by urbanization, and climate change will cause changes in ground surface temperatures. We have provided estimates of ground surface temperature changes in the TCMA in response to land use changes by urbanization and in response to climate change.

Cyclical (seasonal or diurnal) temperature fluctuations at the ground surface drive cyclical temperature fluctuations in the soil below and, if shallow enough, in the groundwater. Seasonal temperature cycles in the ground reach depths on the order of 10 to 15m. Diurnal cycles are confined to the upper 1m or less. The cyclical temperature fluctuations in an unsaturated soil can be modeled with reasonable accuracy by an analytical solution of the 1-D conduction

equation (2.7). For an aquifer (groundwater) layer below an unsaturated soil the solution of the 1-D conduction equation is more complex, because the thermal diffusivities in the aquifer and in the unsaturated soil are vastly different. Equation (3.8) and Figures 3.3, 3.4, and 3.5 can be used to estimate shallow groundwater temperatures due to cyclical surface temperature fluctuations.

Data collected by the MPCA in the St. Cloud, MN area confirm that land use influences groundwater temperatures. Further analysis indicates that a fully urbanized downtown area at the latitude of Minneapolis/St. Paul is likely to have a groundwater temperature that is nearly 3°C warmer than an undeveloped/ agricultural area. Pavements are the main cause of this change.

Global warming will also result in a rise of ground surface temperatures and hence groundwater temperatures. In the extreme case of a $2xCO_2$ climate scenario groundwater temperatures would be expected to rise by up to 4°C.

Seasonal ground water temperature amplitudes would be affected only down to depths of about 10 to 15m. The change in amplitudes would be small at these depths. The groundwater temperature amplitudes depend, to a great degree, on the depth of the groundwater table. If the goal is to measure groundwater fluctuations the depth to the groundwater will be quite important. Fortunately, depth of the groundwater table is one of the easiest of the required parameters to measure.

Compounding urbanization and climate change, by applying the $2xCO_2$ climate scenario to a land use change from “undeveloped” to “fully urbanized”, is expected to raise groundwater temperatures by about 5°C at the latitude of Minneapolis/St. Paul. A mean annual groundwater temperature rise of 5°C would likely have a very adverse affect on trout habitat in many coldwater streams in summer. The mean annual temperature of an undeveloped ground surface in the Twin Cities Region is currently on the order of 11 ^{o}C; it would rise to 16 ^{o}C. Coldwater streams are expected to have water temperatures that do not exceed 20^{o}C by much. If the mean annual temperature is already 16 ^{o}C, this leaves only the narrowest of margins for the natural heating of streams by solar radiation in the summer.

Acknowledgments

This study was conducted with partial support from the Minnesota Pollution Control Agency, St. Paul, Minnesota. Bruce Wilson was the project officer. Soil temperature and climate data used in this study were supplied by several individuals:

1) Dr. David Ruschy, University of Minnesota, Department of Soil, Climate and Water, made available soil and climate data from the St. Paul Weather Observatory.
2) Ben Worel and Tim Clyne, Minnesota Department of Transportation, made available climate and pavement temperature data from the MnROAD site.
3) Mindy Erickson, Minnesota Pollution Control Agency, made available groundwater temperature data from the St. Cloud site.
4) Tim Erickson made available land use data.
5) William Herb made available simulated ground surface temperatures.

We are grateful to these individuals and organizations for their cooperation.

References

Akbari, H., L. S. Rose, and H. Taha. (1999). "Characterizing the Fabric of the Urban Environment: A Case Study of Sacramento, California," LBNL-44688, Lawrence Berkeley National Laboratory, Berkeley, California (December)

Akbari, H. and L. S. Rose. (2001a). "Characterizing the Fabric of the Urban Environment: A Case Study of Salt Lake City, Utah," LBNL-47851, Lawrence Berkeley National Laboratory, Berkeley, California (February)

Akbari, H. and L. S. Rose. (2001b). "Characterizing the Fabric of the Urban Environment: A Case Study of Chicago, Illinois" LBNL-49275, Lawrence Berkeley National Laboratory, Berkeley, California (October)

Asaeda, Takashi and Ca, Vu Thanh (1993). "The Subsurface Transport of Heat and Moisture and its Effects on the Environment: A Numerical Model" *Boundary-Layer Meteorology* 65: 159-179

Baker, J.M., and D.G. Baker (2002). "Long-term ground heat flux and heat storage at a mid-latitude site". *Climatic Change* 54:295-303.

Baehr, H.D. and Stephan, K. (2006). *Heat and Mass Transfer – Second Edition*. Springer, Berlin Heidelberg, New York, 688pp.

Bear, J. (1972). *Dynamics of fluids in porous media.* American Elsevier Publishing Company, Inc., New York, 764pp.

Benekos, D.I. (2005). “On the determination of transverse dispersivity: Experiments and simulations in a helix and a cochlea”. PhD dissertation, Department of Civil and Environmental Engineering, Stanford University, 122 pp.

Boer, G.J., McFarlane, N.A., Lazare, M. (1992). “Greenhouse gas –induced climate changesimulated with the CCC Second-Generation General Circulation Model”. *J. Climate* 5(10): 1045-1077.

De Vries, D.A. (1966) “Thermal Properties of Soils”. Physic of Plant Environment, Van Wijk, W.R. (ed.) Amsterdam pp.210-230.

Erickson, Timothy and Stefan, Heinz G. (2008) “Groundwater Recharge from a Changing Landscape”. Project Report No 490 Anthony Falls Laboratory, University of Minnesota, Minneapolis, MN, 112pp

Fang, X. and Stefan, H.G. (2004). “Simulation of thermal/dissolved oxygen habitat for fishes in lakes under different climate scenarios. Part 1. Cool water fish in the contiguous U.S.” *Ecological Modelling* 172 (2004): 13-37.

Herb, W. R., Janke, B., Mohseni, O. and Stefan, H.G. (2006). “All-Weather Ground Surface Temperature Simulation”. Project Report No. 478 St. Anthony Falls Laboratory, University of Minnesota, Minneapolis, MN, 57pp.

Herb, W. R., Janke, B., Mohseni, O. and Stefan, H.G. (2007). “Estimation of Runoff Temperatures and Heat Export from Different Land and Water Surfaces” Project Report No. 488, St. Anthony Falls Laboratory, University of Minnesota, Minneapolis, MN, 34pp.

Hoffmann, Klaus A. and Chiang, Steve T. (2004) *Computational Fluid Dynamics Volume I Fourth Edition*. Engineering Education System, Wichita, Kansas

Hondzo, Midhat and Stefan, Heinz G. (1993) “Lake Water Temperature Simulation Model”. *Journal of Hydraulic Engineering* Vol.119, No. 11, pp.1251-1273.

IPCC (2007). Summary for Policymakers, WGI Fourth Assessment Report
Page 11 of 21

Kersten, M.S. (1948) “The Thermal Conductivity of Soils”. *Proceedings of Highway Research Board,* Vol.28, pp.391-409.

Minnesota Pollution Control Agency (MPCA) (2001). “Effects of Land Use on Ground Water Quality, St. Cloud Area, Minnesota – Summary of Results from 1997 through 2000” Ground Water Monitoring and Assessment Program”. 66 pp.

Paringit, Enrico C. and Nadaoka, Kazuo. (2003). "Sediment yield modelling for small agricultural catchments: land-cover parameterization based on remote sensing data analysis" *Hydrological Processes* 17, 1845-1866

Rose, Leanna Shea., Akbari, Hashem., and Taha,Haider. (2003). "Characterizing the Fabric of the Urban Environment: A Case Study of Greater Houston, Texas" LBNL-51448, Lawrence Berkeley National Laboratory, Berkeley, California (January)

Taniguchi, Makoto and Uemura, Takeshi. (2005). “Effects of urbanization and groundwater flow on the subsurface temperature in Osaka, Japan” *Physics of the Earth and Planetary Interiors* 152, 305–313

USEPA and USDOE “ENERGY STAR® Program Requirements for Programmable Thermostats” Eligibility Criteria (Version 1.2). <http://www.energystar.gov/ia/partners/product_specs/eligibility/thermostats_elig.pdf>

Zheng, C. and Bennett, G.D. (1995). *Applied contaminant transport modeling: theory and practice.* Van Nostrand Reinhold. New York.

Appendix A: Thermal diffusivity of soils

Many sources only report a soil's thermal conductivity (κ). Thermal diffusivity is directly related to thermal conductivity, density (ρ) and specific heat (c_p).

$$\alpha = \frac{\kappa}{\rho \cdot c_p} = \frac{\kappa}{C} \tag{A.1}$$

The terms in the denominator of equation (A.1) constitute the heat capacity of the soil. De Vries (1966) shows that the heat capacity of a soil can be determined from its constituents.

$$C_i = \rho_i \cdot c_{pi} \tag{A.2}$$

$$C = V_s \cdot C_s + V_w \cdot C_w + V_a \cdot C_a \tag{A.3}$$

where: C = heat capacity (Sub-script denotes material)
V_s, V_w, and V_a = volume fractions solids, water, and air respectively

De Vries (1966) provides tables of heat capacity, specific heat and density of various materials. Tables A.1 and A.2 include this data converted into convenient units.

Table A.1 Heat capacity (C) of water and air

Material	C ($J/m^3/°C$)
Water	4186800
Ice	1884060
Air	1256

Table A.2 Specific heat and density of various geo-materials

Material	c_s (J kg^{-1} °C^{-1})	Mean Temp. (°C)	ρ_s (kg/m^3)
Soil			
Northway fine sand	824.80	61	2760
Northway sand	715.94	-6.7	2740
	774.56	18.8	
	799.68	60.2	
Northway silt loam	703.38	-10.4	2700
	736.88	20.1	
	808.05	60.4	
Chena river gravel	812.24	61	2700
	820.61	60.4	
Fairbanks silt loam	686.64	-8.4	2700
	766.18	18.8	
	812.24	61.3	
Graded Ottawa sand	657.33	-9.5	2650
	686.64	18.5	
	736.88	37.7	
	791.31	60.3	
23-30 Ottawa sand	766.18	37.8	2650
	791.31	59.9	
Lowell sand	665.70	-9.5	2670
	787.12	19.7	
	787.12	60.9	
Crushed quartz	795.49	60.9	2650
Crushed trap rock	808.05	59.9	2970
Crushed feldspar	795.49	59.3	2560
Crushed granite	674.07	-13.3	2670
	728.50	19.4	
	791.31	60.9	

Material	c_s (J kg^{-1} °C^{-1})	Mean Temp. (°C)	ρ_s (kg/m^3)
Organic Material			
Humus	1997.10	--	1260
	1854.75	~60	
"Verwitterungserde"	1741.71		
"Bolster"	1925.93	28	1360
Soil Minerals and Rock Materials			
Quartz	799.68	~60	2650
Kaolin	937.84	~60	2600
$CaCO_3$	870.85	~60	2710
$MgCO_3$	1029.95	~60	3040
$CaSO_4$	816.43	~60	2450
Fe_2O_3	690.82	~60	5240
Al_2O_3	908.54	--	3700
$Fe(OH)_3$	946.22	~60	3600
Orthoclase	812.24	~60	2560
Oligoclase	858.29	~60	2640
Potash mica	870.85	~60	2900
Magnesia Mica	862.48	~60	2900
Hornblende	816.43	~60	3200
Apatite	808.05	~60	3200
Dolomite	929.47	~60	2900
Talc	875.04	~60	2700
Granite	803.87	56	2600
Syenite	833.17	59	2700
Diorite	812.24	65	2900
Andesite	833.17	59	2400
Basalt	891.79	55	3000

Kersten (1948) developed a series of equations to predict the thermal conductivity of soil based on density and moisture content. Note that conversion factors have been added to Kersten's original equations in order to produce more desirable units.

For unfrozen, silt and clay soils:

$$\kappa = 3844.05 * (0.9Log(M.C.) - 0.2)10^{(0.000624\rho)} \quad \text{(A.4)}$$

For unfrozen, sand soils:

$$\kappa = 3844.05 * (0.7Log(M.C.) + 0.4)10^{(0.000624\rho)} \quad \text{(A.5)}$$

For frozen, silt and clay soils:

$$\kappa = 3844.05 * \left[0.01(10)^{(0.00132\rho)} + 0.025M.C.(10)^{(0.000874\rho)}\right] \quad \text{(A.6)}$$

For frozen, sand soils:

$$\kappa = 3844.05 * \left[0.011(10)^{(0.00134\rho)} + 0.026 M.C.(10)^{(0.000912)}\right] \qquad \text{(A.7)}$$

where: κ = thermal conductivity (J /m /day /°C)
$M.C.$ = moisture content expressed as a percent of the dry weight of the soil (%)
ρ = dry soil density (kg/m^3)

Kersten (1948) defines a silt/clay soil as a soil with more than 50% silt/clay content. Kersten (1948) also notes that the sand soils used to develop equations (A.4) through (A.7) were relatively clean, and for sandy soils with high silt/clay content (~40%) an interpolation of the silt/clay and sand equations should be used.

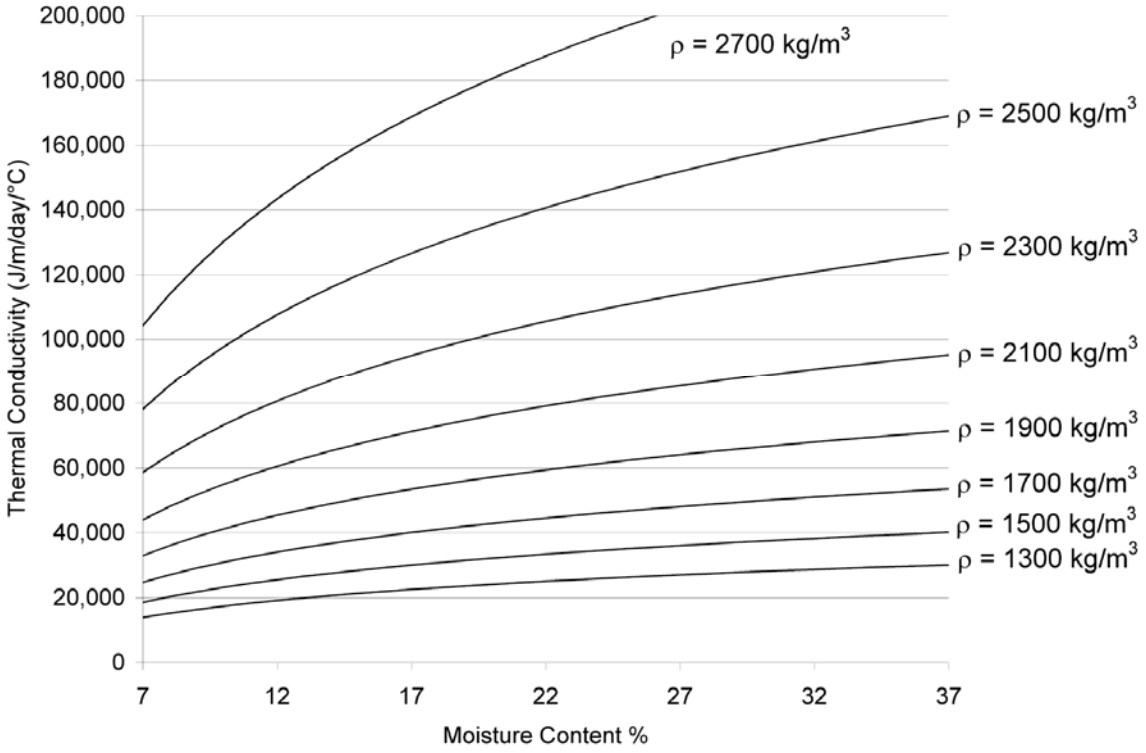

Figure A.1 Thermal conductivity of (unfrozen) silt and clay soils

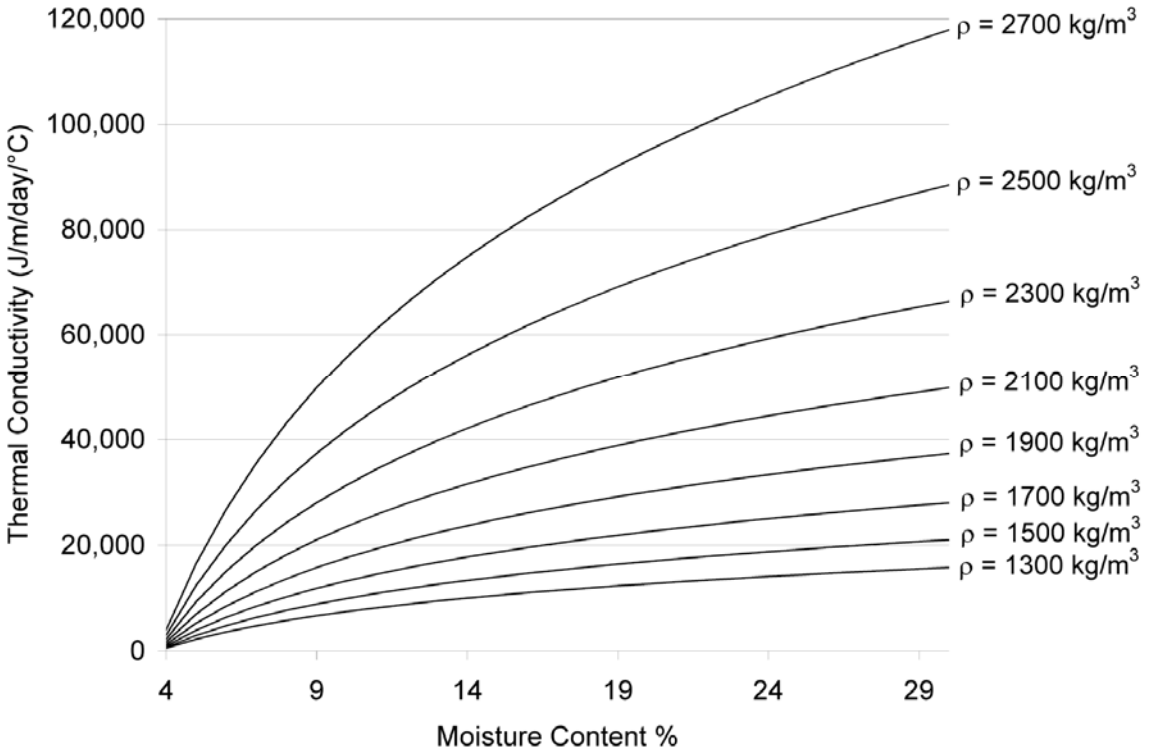

Figure A.2 Thermal conductivity of (unfrozen) sand soils

When the soil is fully saturated the moisture content can be calculated based on the porosity (n) of the soil, the dry soil density (ρ), and the density of water (ρ_w).

$$M.C._{sat} = 100 * n \frac{\rho_w}{\rho} \tag{A.8}$$

Equation (A.9) also provides a useful translation between moisture content and percent saturation.

$$\%Saturation = 100 \frac{M.C.}{M.C._{sat}} = M.C. \frac{\rho}{n \cdot \rho_w} \tag{A.9}$$

Appendix B: Thermal diffusivity in an aquifer

In an aquifer where groundwater is moving horizontally, vertical thermal diffusivity (α) is related to the coefficient of transverse hydrodynamic dispersion or dispersivity (α_T). Figure B.1, a copy of Figure 10.4.1 in Bear (1972), provides a relationship between diffusivity and longitudinal hydrodynamic dispersion. Figure B.2 is an adaptation of Figure 10.4.1 from Bear (1972) and can be described by equations (B.2) and (B.3).

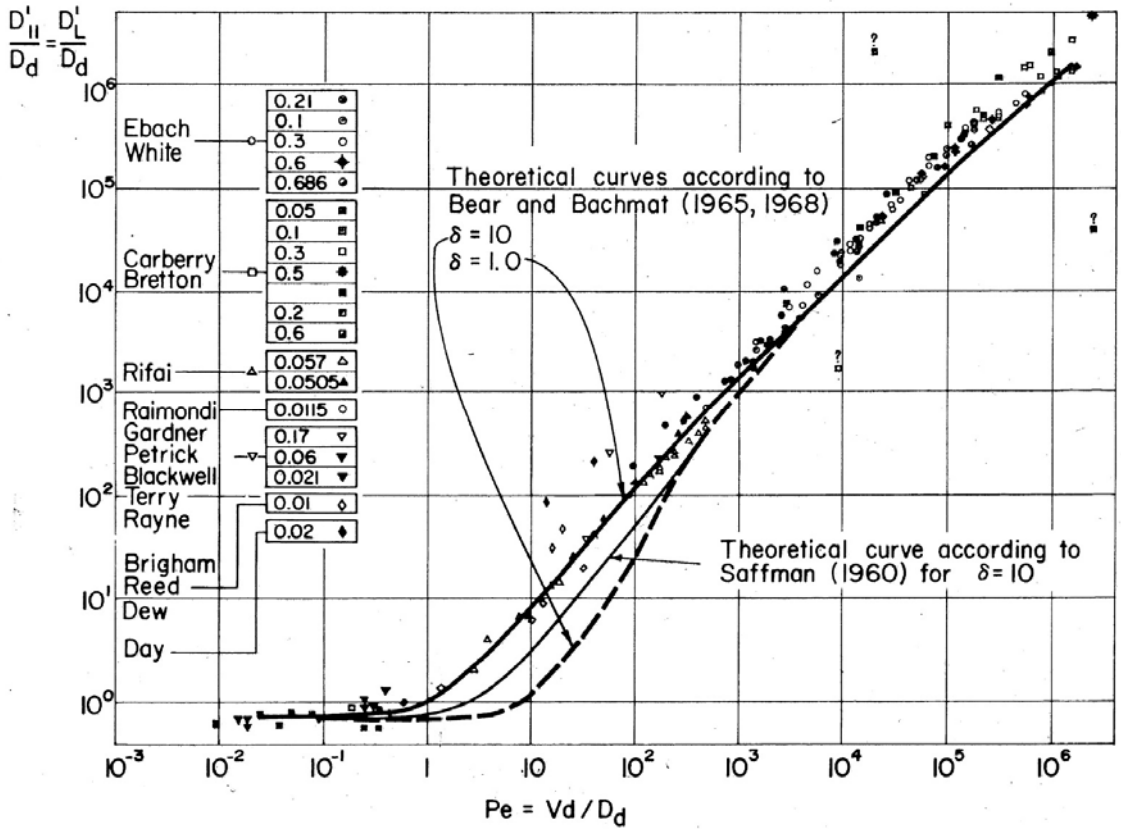

Figure B.1 Bear (1972) relationship between (longitudinal) hydrodynamic dispersion coefficient D_L and molecular diffusivity D_d as a function of Peclet number $Pe = Vd/D_d$ (after Pfannkuch). V = Darcy velocity in the porous medium, and d = grain size

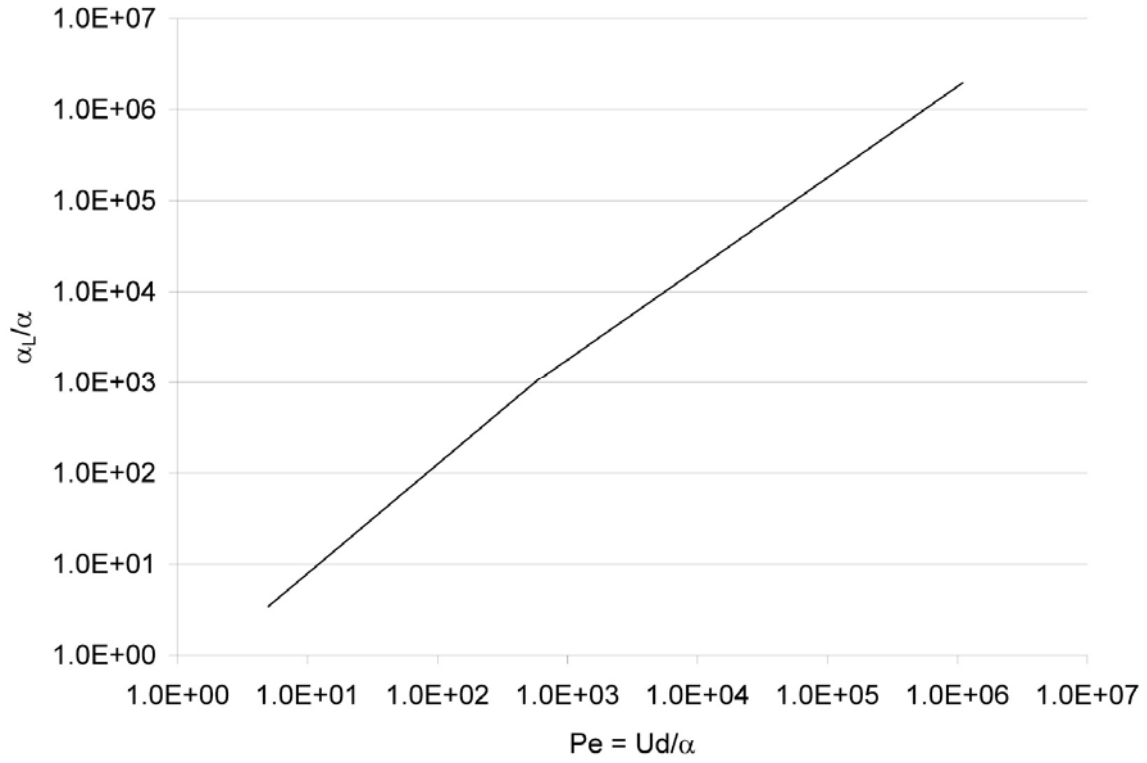

Figure B.2 Longitudinal hydrodynamic dispersion coefficient α_L / α as a function of the thermal Peclet number (*Pe*)

$$Pe \equiv \frac{U \cdot d}{\alpha} \tag{B.1}$$

where U = Darcy velocity
d = mean grain size
α = thermal diffusivity

The longitudinal dispersion coefficient (α_L) can be approximated

for Pe < 600 as

$$\frac{\alpha_L}{\alpha} = 0.5(Pe)^{1.2} \tag{B.2}$$

for Pe > 600 as

$$\frac{\alpha_L}{\alpha} = 1.8Pe \tag{B.3}$$

Note that Bear (1972) defines Peclet number with mass diffusivity; whereas, Baehr and Stephan (2006) define Peclet number with thermal

diffusivity. We imply that Reynolds' analogy can be used, i.e. thermal diffusivity and mass diffusivity are the same.

In first approximation the relationships for the (longitudinal) dispersion coefficient of mass can therefore be applied to estimate transverse thermal diffusivity. Benekos (2005) reports that the ratio of transverse dispersivity to longitudinal dispersivity ranges from one-half to one-third. Based on this information, it is our recommendation to use a ratio of α_T/α_L = 1/3 to predict transverse hydrodynamic dispersion from longitudinal dispersion; however, hydrodynamic dispersion should not be less than molecular thermal diffusivity. Zheng and Bennett (1995) and Qian (2007) also used α_T/α_L = 1/3.

In actuality dispersion is a tensor with α_{xx}, α_{xz}, α_{zz}, α_{zx}. Zheng and Bennett (1995) provide a relationship between these tensor terms and longitudinal and transverse dispersion (equations B.4 – B.6). An equation for dispersive flux is also provided (B.7). Although the tensor form of dispersion is more accurate for two-dimensional conduction modeling, the one-third ratio between transverse and longitudinal dispersion is still a good approximation when estimating hydrodynamic dispersion within the accuracy that is necessary for these types of problems.

$$\alpha_{xx} = \alpha_L \frac{v_x v_x}{|V|} + \alpha_T \frac{v_y v_y}{|V|} \tag{B.4}$$

$$\alpha_{xy} = \alpha_{yx} = \alpha_L \frac{v_x v_y}{|V|} - \alpha_T \frac{v_y v_x}{|V|} = (\alpha_L - \alpha_T)\frac{v_x v_y}{|V|} \tag{B.5}$$

$$\alpha_{yy} = \alpha_L \frac{v_y v_y}{|V|} + \alpha_T \frac{v_x v_x}{|V|} \tag{B.6}$$

$$\begin{bmatrix} q_x \\ q_y \end{bmatrix} = -\begin{bmatrix} \alpha_{xx} & \alpha_{xy} \\ \alpha_{yx} & \alpha_{yy} \end{bmatrix} \begin{bmatrix} \dfrac{\partial T}{\partial x} \\ \dfrac{\partial T}{\partial y} \end{bmatrix} \tag{B.7}$$

where: v_x = x-component of velocity
v_z = z-component of velocity
$|V|$ = velocity magnitude
q_x = x-component flux
q_z = z-component flux

It should be noted that Bear's (1972) analysis assumes that the "tracer" does not affect the fluid properties. In this case the tracer is temperature, which does in fact affect the density of the groundwater. Assuming the groundwater is

warmer than 4°C, the warmer water will be less dense. The buoyancy of the warmer water, infiltrating from the top, will reduce transverse (vertical) mixing and decrease the thermal diffusivity in the groundwater.

Appendix C: Analytic model for vertical heat conduction into shallow groundwater

It is temping to apply the solutions given for a uniform soil to describe the vertical temperature profile in the groundwater. As discussed earlier this method is incorrect because it violates the uniform soil assumption. A boundary condition translation method of applying the uniform soil solution is explored in this appendix to provide an example of how greatly this method can underestimate the damping at the groundwater table.

The temperature fluctuations at the top of the groundwater table will first be calculated using the analytic solution for a uniform soil. These fluctuations will then be used as the new boundary condition for the domain within the groundwater.

Begin with equations (2.4) and (2.7). These will apply to the region above the groundwater table.

For $z < S$:

$$T^* = e^{-2\pi z/\Lambda_s} \cos\left(2\pi\left(\frac{t}{t_0} - \frac{z}{\Lambda_s}\right)\right) \tag{C.1}$$

$$T^* = \frac{T(z,t) - T_m}{\Delta T} \tag{C.2}$$

$$\Lambda_s = 2\sqrt{\pi \alpha_s t_0} \tag{C.3}$$

For $z = S$:

$$T^* = e^{-2\pi S/\Lambda_s} \cos\left(2\pi\left(\frac{t}{t_0} - \frac{S}{\Lambda_s}\right)\right) \tag{C.4}$$

Where: T_s = temperature at surface of groundwater table

Define:

$$\Delta T_s \equiv \Delta T e^{\left(\frac{-2\pi S}{\Lambda_s}\right)}$$
$$\frac{t_s}{t_{0s}} \equiv \frac{t}{t_0} - \frac{s}{\Lambda_s} \tag{C.5}$$

Equations (C.4) and (C.5) combine to:

$$T_s = T(s,t) = T_m + \Delta T_s \cos\left(2\pi \frac{t_s}{t_{0s}}\right) \tag{C.6}$$

Where: T_s = temperature at surface of groundwater table

Use (C.7) as the boundary condition for $z > S$.

For $z > S$:
$$\frac{T(z,t)-T_m}{\Delta T_s} = e^{-2\pi(z-S)/\Lambda_2}\cos\left(2\pi\left(\frac{t_s}{t_{0s}}-\frac{(z-S)}{\Lambda_g}\right)\right) \quad \text{(C.7)}$$

$$\Lambda_g = 2\sqrt{\pi\alpha_g t_0} \quad \text{(C.8)}$$

Substituting the (C.8) definitions yields:

$$\frac{T(z,t)-T_m}{\Delta T e^{\left(\frac{-2\pi S}{\Lambda_s}\right)}} = e^{-2\pi(z-S)/\Lambda_g}\cos\left(2\pi\left(\frac{t}{t_0}-\frac{S}{\Lambda_s}-\frac{(z-S)}{\Lambda_g}\right)\right) \quad \text{(C.9)}$$

Substituting (C.2) into (C.9) and rearranging yields:

$$T^* = e^{-2\pi\left(\frac{S}{\Lambda_s}\left(1-\frac{\Lambda_s}{\Lambda_g}\right)+\frac{\Lambda_s}{\Lambda_g}\left(\frac{z}{\Lambda_s}\right)\right)}\cos\left[2\pi\left(\frac{t}{t_0}+\frac{S}{\Lambda_s}\left(\frac{\Lambda_s}{\Lambda_g}-1\right)-\frac{\Lambda_s}{\Lambda_g}\left(\frac{z}{\Lambda_s}\right)\right)\right] \quad \text{(C.10)}$$

Combining equations (C.1) and (C.10) provides a conditional temperature solution for all depths. Note that these equations are the same as equations (3.8) and (3.9).

$$\begin{aligned} T_u &= G(s-z)*e^{-2\pi z/\Lambda_1}\cos\left(2\pi\left(\frac{t}{t_0}-\frac{z}{\Lambda_1}\right)\right)+\cdots \\ &\cdots G(z-s)*e^{-2\pi\left(\frac{S}{\Lambda_s}\left(1-\frac{\Lambda_s}{\Lambda_g}\right)+\frac{\Lambda_s}{\Lambda_g}\left(\frac{z}{\Lambda_s}\right)\right)}\cos\left[2\pi\left(\frac{t}{t_0}+\frac{S}{\Lambda_s}\left(\frac{\Lambda_s}{\Lambda_g}-1\right)-\frac{\Lambda_s}{\Lambda_g}\left(\frac{z}{\Lambda_s}\right)\right)\right] \end{aligned} \quad \text{(C.11)}$$

where: $G(y) = \begin{cases} 1, y \geq 0 \\ 0, y < 0 \end{cases}$

The analytic model given in equation (C.11) is for an infinitely deep aquifer while the numeric solution provided in section 2.1 has an adiabatic boundary at the base of the aquifer. In order to make a comparison between the analytic and the numeric, the analytic solution needs to have an adiabatic lower boundary imposed. This is accomplished by a thermal reflection at the lower boundary. A thermal reflection can be modeled by the method of images. Equation (C.11) is used to model the non-reflected temperature penetration. The z term in equation (C.11) is redefined to model the reflected image. The two equations for the real heat source at z=0, and the image heat source at a depth z=2(S+h) are then

added and result in equation (C.12). Figure 3.6 is a diagram of the non-reflected temperature penetration and its reflected image.

$$T_R^* = T^*(z,t) + T^*(2(S+h) - z,t) \qquad \text{(C.12)}$$

where T^*_R = soil or groundwater temperature with reflection at bedrock
h = thickness of the aquifer

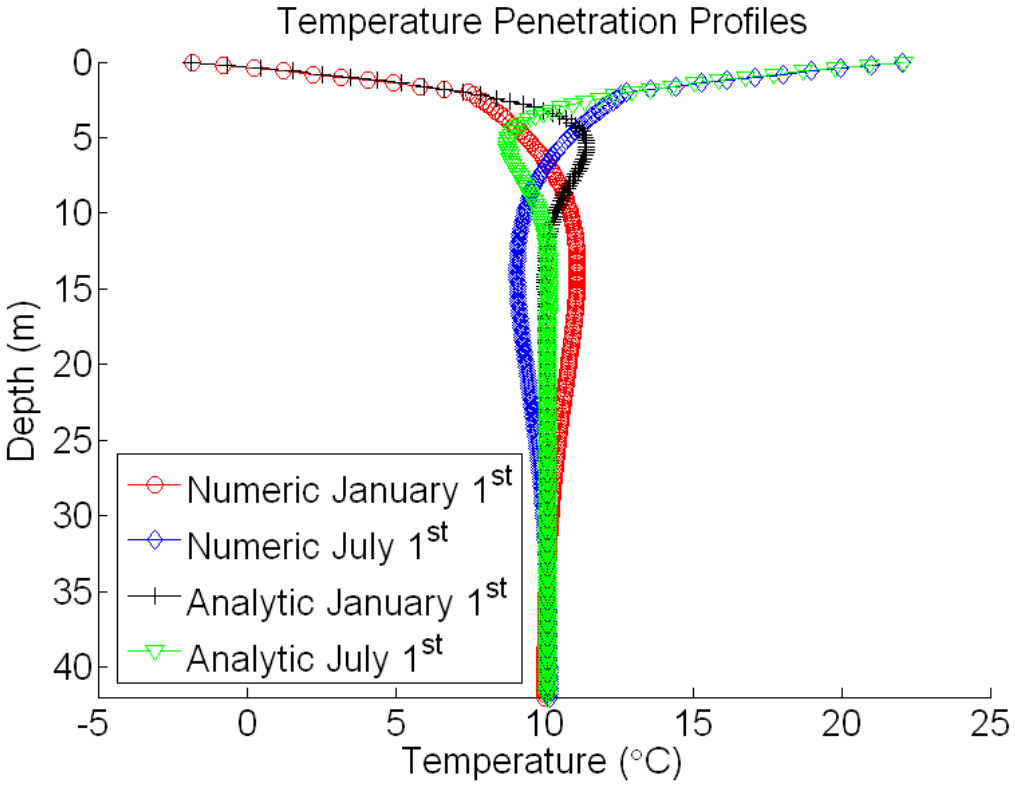

Figure C.1 Example from Figure 3.2 to demonstrate the differences in temperature profiles generated by the analytic and numeric solutions

Appendix D. Future data needs

Very little data is available to verify groundwater heat transport models. Additional data is needed both for verification of the concepts discussed and for future groundwater heat transport research.

Future research interests may include: steady or unsteady groundwater transport downstream from a detention pond or infiltration source, the effects of unsaturated infiltration on heat transport, transport in the unsaturated flow region (the fringe), the relationship between soil temperatures and groundwater temperatures, and the effects of buoyant thermal plums on dispersivity.

There are several types of site conditions and equipment/instrumentation of interest. The primary goals of most instrumental setups would be to measure the temperature profile from the surface down and to determine the groundwater depths and flow characteristics. Well nests commonly used in current monitoring practice can provide groundwater depths and flow characteristics. It would be possible to establish a temperature profile by placing thermistors in the bottom of several well points driven to different depths. It would, however, be preferable to have all to the thermistors in the same monitoring well. This would require a single well with multiple screens. Figure D.1 gives the concept of a multi-screen well for this purpose. Each screen would contain one sensor and would be separated by a length of well casing and physical barrier. A pressure gage would also be needed in one of the screens in order to determine the depth to the groundwater surface. The objective of the barrier is to prevent mixing inside the well casing between the sampling points. The physical barrier could consist of a washer welded or glued into place, a rubber plug, an expanding plug, or expanding foam. A PVC well casing is preferable to a metal one because a metal casing could act as a thermal conduit from the surface down, however, insulating the exposed portion of the well would help reduce this effect.

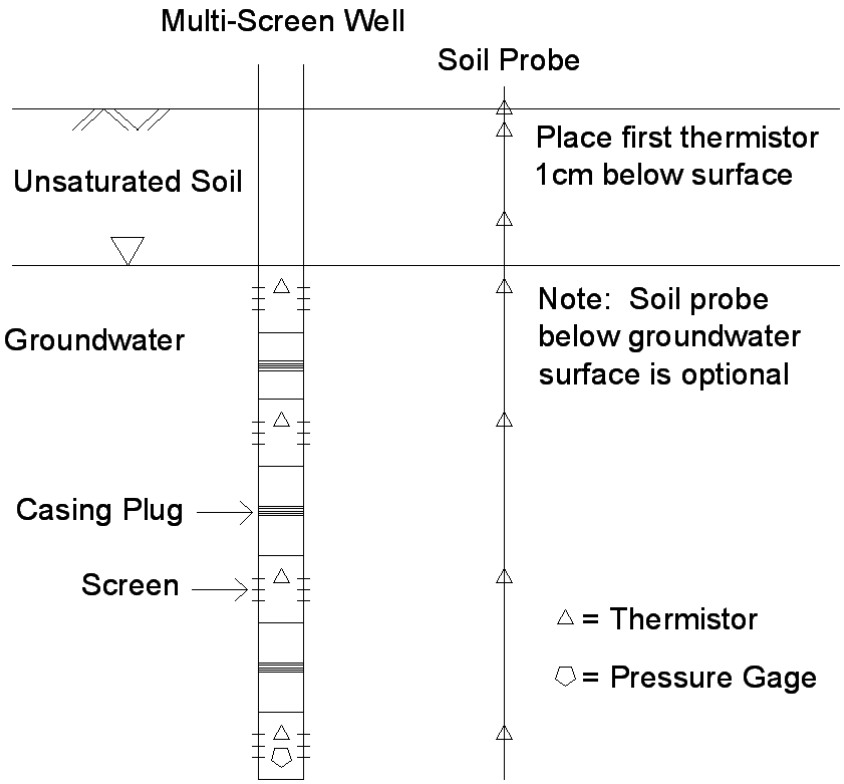

Figure D.1 Diagram of multi-screen monitoring well system

Other measurements to be considered are surface and soil temperatures, rainfall rates, and runoff/infiltration rates. The surface and soil temperature measurements are curial for establishing a temperature profile. The rainfall, runoff, and, infiltration rates are more important for sites near detention ponds and recharge sources.

Temperature profile data from shallow aquifers would be valuable; data from several sites would most telling. A site with a fairly stable shallow groundwater table would set a good base line. A line of monitoring wells perpendicular to a straight river would also provide a good set of base line data. At these base line sites soil temperature gages at several depths and wells with thermistors should be placed. This would provide information on the relationship between soil and groundwater temperatures. Wells near wet detention ponds and near infiltration basins can provide information on heat transport by infiltrating water. Monitoring wells between a detention pond and a stream can provide temperature data would be useful for verifying mixing zone models.